Chapter 14
Structural Characterization of Amorphous Solid Dispersions

Amrit Paudel, Joke Meeus and Guy Van den Mooter

14.1 Introduction

Amorphous solid dispersions (ASD) consist of active pharmaceutical ingredient (API) molecules dispersed in stabilizing carrier(s) which are mostly amorphous polymers along with some functional excipients and are powder, extrudates, thin films, porous foams, surface-coated beads, etc. (Paudel et al. 2013). Hygroscopicity of amorphous materials as well as the carriers increase the analytical complexity (Palermo et al. 2012a, b). Additional excipients further complicate the characterization of amorphous systems in the finished dosage form. The comprehensive qualitative/quantitative characterization of molecular mobility, miscibility, phase separation, domain size, crystallinity, surface chemistry, moisture/solvent, molecular interactions in ASD requires a gamut of analytical techniques. Calorimetric techniques (differential scanning calorimetry (DSC), isothermal microcalorimetry (IMC), and localized thermal analysis) are common for the analysis of ASD (Baird and Taylor 2012). Dielectric spectroscopy and thermomechanical techniques are also increasingly used for the ASD analysis. Infrared, Raman, and solid-state nuclear magnetic resonance spectroscopy (SS-NMR) analyze the molecular interactions among the components of ASD and structural changes during phase separation/crystallization and quantify crystallinity (Vogt and Williams 2010). Polarized light microscopy, scanning/transmission electron microscopy, and atomic force microscopy (AFM) probe the morphological characteristics, spatial phase distribution, and crystallinity. Powder X-ray diffraction is selective for detecting/quantifying the crystallinity (Vogt and Williams 2010). X-ray photoelectron scattering (Dong and Boyd 2011), inverse gas chromatography (IGC) and time-of-flight secondary ion mass spectrometry (Ho and Heng 2013; Barnes et al. 2011) are highly sensitive

G. Van den Mooter (✉) · A. Paudel · J. Meeus
Drug Delivery and Disposition, University of Leuven, Leuven, Belgium
e-mail: Guy.Vandenmooter@pharm.kuleuven.be

A. Paudel
Research Center Pharmaceutical Engineering GmbH (RCPE), Graz, Austria

N. Shah et al. (eds.), *Amorphous Solid Dispersions,*
Advances in Delivery Science and Technology, DOI 10.1007/978-1-4939-1598-9_14

and/or selective to ASD surface analysis. Gravimetric vapor sorption (GVS) probes the hygroscopicity, crystallinity/crystallization and drug–polymer interactions (Burnett et al. 2009). Thermogravimetric analysis measures the moisture and/or volatile content in ASD. The use of multiple simultaneous measurement tools for the integrated information with a spatiotemporal resolution is increasing. This chapter focuses on the thermal, diffractometric, and moisture sorption analysis of amorphous pharmaceuticals.

14.2 Differential Scanning Calorimetry (DSC) Studies of ASD

Non-isothermal DSC involves the controlled heating and/or cooling of a material in a DSC sample holder (pan) along with a reference (usually an empty pan) inside a furnace supplied with a constant flow of inert gas and a cooling system. In a heat flux setup, the temperature difference between the sample and the empty reference pan placed inside the same furnace is measured by separate thermocouples as a function of temperature. In contrast, the instrumental output is the electrical power difference between the sample and the reference pan housed inside the isolated furnace in case of a power-compensation DSC. The heat flow evolved from or transferred in the sample is derived from the measured temperature or power difference as the end response. DSC also enables measurement of isothermal crystallization kinetics. Various endothermic events/transitions such as glass transition, melting, desolvation, enthalpy recovery and some degradation reactions absorb heat while the exothermic processes viz., crystallization, crystal perfection, and some thermal decomposition liberate heat from the sample. A DSC thermogram obtained by heating or cooling at linear rate includes the heat-capacity (C_P)-related transitions and kinetic events. Thus, the total heat flow (THF) signal recorded by DSC (dQ/dt) can be presented as:

$$\frac{dQ}{dt} = C_p.\beta + f(t, T), \tag{14.1}$$

where *t, T,* and β are the time, temperature, and heating rate, respectively. The first term in the right hand side is the C_p-related heat flow and the second the kinetic heat flow. The multiple transitions occurring concomitantly in DSC traces pose challenges in qualitative and quantitative interpretation. One way of improving this is superimposing a nonlinear heating/cooling program on the linear temperature program, prevalently called modulated temperature DSC (mDSC). A single frequency sinusoidal oscillation is the most used nonlinear heating in mDSC setup for pharmaceutical solid dispersions. The expression for dQ/dt, in case of mDSC, can be rewritten as:

$$\frac{dQ}{dt} = C_P.\left[\beta + A_T.\omega.\cos(\omega.t)\right] + f'(t, T) + A_K.\sin(\omega.t) \tag{14.2}$$

where A_T and $\omega(= 2\pi/\text{modulation period } (p))$ are respectively the amplitude and the angular frequency of temperature modulation and β is the linear heating rate.

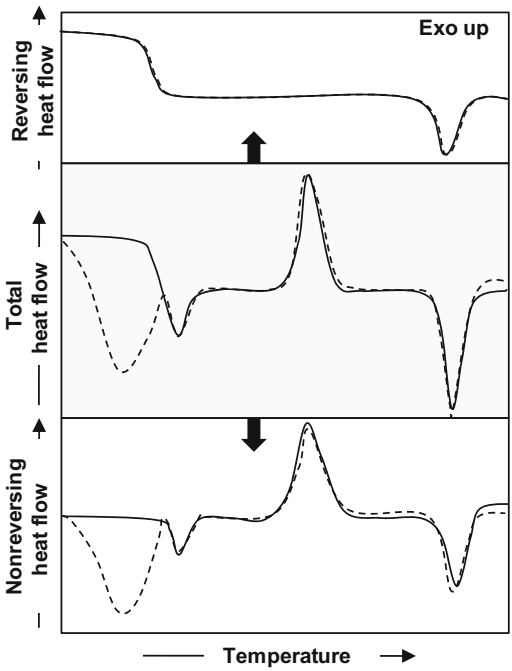

Fig. 14.1 Characteristic mDSC thermograms of amorphous solids undergoing non-isothermal crystallization (*solid line*) and the same of the amorphous solid containing moisture (*dashed line*)

Here, $f'(t, T)$ represents the kinetic component without temperature modulation while A_K is the amplitude of kinetic response to the temperature modulation. In this way, the measured frequency-dependent heat capacity in addition to the total heat capacity makes it possible to deconvolute the THF signal into the reversing (C_p related) and nonreversing (kinetic) heat flow components. Reversing heat flow (RHF) usually comprises all transitions that are thermodynamically reversible at the temperature and the time they are measured, e.g., glass transition and melting. In contrast, nonreversing heat flow (NRHF) which is obtained by subtraction of RHF from THF, consists of transitions nonreversible at the temperature and time of the measurement such as enthalpic recovery, cold crystallization, evaporation, desolvation, thermal decomposition, curing, etc. A typical mDSC thermogram for an amorphous material undergoing non-isothermal crystallization is depicted in Fig. 14.1. The dashed line represents an amorphous material containing some moisture and/or volatile solvent. The first event exhibiting the step jump in RHF is the glass transition of the material. The accompanying endothermic overshoot from the baseline in THF is originated from the overlapping enthalpy recovery signal and additional broad endotherm is from desolvation, both apparent in NRHF. The exothermic peak is of the cold crystallization and the final endotherm is of melting.

Various experimental conditions crucially affect the resultant heat flow measured by DSC, e.g., sample size, pan and purge gas type, sample–pan contact, the heating/cooling rate. The increase in the scan rate proportionally improves the sensitivity while inversely affect the resolution. Many times, fast heating or cooling rates are

preferred to kinetically enhance the desirable event in DSC. Heating or cooling at a rate that is considerably faster than the time scale of the process of interest, using fast scan DSC, hyper DSC or flash DSC, can be helpful to obtain reliable calorimetric data about the initial material structure (Ford and Mann 2012). Fast cooling can be advantageous for in situ amorphization for rapidly crystallizing materials. Ideally, the fast heating enhances the weak glass transition signals or for detecting the glass transition of thermally unstable materials which start degrading prior to its T_g. For high scan rate, the sample size and thickness need to be extremely small and thermal contact should be excellent to avoid thermal gradient and lag (Zhuravlev and Schick 2010). The mDSC signals rely on the combinations of β, A_T, and ω (Santovea et al. 2010). For example, heat-iso amplitude ($\beta = A_T.\omega$) is suitable for studying melting/crystallization. For amorphous blends, where various transitions are expected heating–cooling mode ($\beta < \mathrm{A_T}.\omega$) is more preferred. Great caution is needed while choosing the combinations of β, A_T, and p so that the applied program can be followed by the sample. At least four to six cycles across each transition ensure efficient signal deconvolution. The "p" is selected according to the C_P of a material and the width of transitions such that the lower the C_P, the lower is the period required while the wider the transition, the higher is the period required. Higher A_T generally increases sensitivity and decreases resolution. The plot of modulated heat flow as a function of temperature, propagating as a smooth regular sine wave indicates the optimal combination of mDSC parameters, while the distorted profile suggests the improper modulation parameters. Lissajous plot, the modulated heat flow versus the modulated heating rate, can diagnose the stability of modulation condition, the distortion indicating the uncontrolled condition. The width and the slope of a Lissajous coil represent the phase lag and the C_P, respectively. The amplitude of the periodic function changes across the C_P -related transition retracing the eccentricity of ellipse.

14.2.1 Glass Fragility, Molecular Mobility, and Enthalpy Recovery

The heat capacity difference measured between glass and supercooled liquid (ΔC_P), the position as well as the shape of T_g describe the dynamics of amorphous systems. In general, amorphous polymers behave as strong glasses that exhibit quasi-Arrhenius behavior of viscosity and structural relaxation time often yieldinga broad glass transition (larger T_g width; ΔT_g) with relatively small ΔC_P. The ratio of T_g to melting temperature (T_m) exceeds significantly to 2/3. On the other hand, most of small molecular weight APIs are fragile glasses that significantly deviate from the Arrhenius path in the T_g region, thus show a sharp T_g and T_g/T_m often below 2/3. The ΔT_g measured during heating or cooling in DSC can thus be correlated to the apparent activation energy for molecular motion at T_g (Moynihan 1993). Hancock et al. 1998 tested this relationship on various sugars, indomethacin, and polyvinylpyrrolidone (PVP) with different molecular weights. Kawakami (2011) estimated the size of the

cooperatively rearranging region of glassy ribavirin as a function of sub-T_g annealing time using the ΔT_g.

The fragility (m), the extent of deviation from Arrhenius behavior, of a material can be estimated from a series of T_g's obtained under different heating/cooling rates. An empirical relation of m with DSC data ($= 56 \times T_g \Delta C_P / \Delta H_m$) was proposed by Wang et al. (2002) for many glasses. The derived parameters from DSC data correlate with the crystallization tendency of some amorphous APIs (Kawakami et al. 2012). For indomethacin/PVP ASD, it was reported that the fragility parameters deducted from DSC data considerably differ for the dispersions prepared from different routes viz., the values of "m" were in the order of melt quenching > spray drying > ball milling (Ke et al. 2012). The configurational entropy was unable to predict nonequilibrium glass stability (Graeser et al. 2009).

DSC is the most used technique to study the molecular mobility of amorphous pharmaceuticals at and below T_g. The higher molecular mobility of the glassy state of amorphous systems approaches towards the virtual structural equilibrium through molecular densification and the loss of the free volume and enthalpy with time. The process is called structural or enthalpy relaxation. The primary process, referred to as α-relaxation, originates from the cooperative global mobility of entire structure or segmental motion. It has been shown that the α-process is the main precursor for crystallization (Caron et al. 2010). The temperature dependence of this global mobility below T_g can be described using the Adam–Gibbs–Vogel (AGV) expression, and the non-Arrhenius behavior of the same across glass transition region can be described using Vogel–Fulcher–Tammann (VFT) law (Greco et al. 2012). The Arrhenius-type secondary relaxations evolve from local motions mostly intramolecular, rotational motions of a nonrigid molecular fragment, the common being a β-process. This faster motion has been found responsible for the crystallization of some drugs below T_g and also as the precursor for global mobility (Bhattacharya and Suryanarayanan 2009). It is also possible for molecules to possess multiple secondary processes.

The molecular domains in amorphous structure behave like an ensemble of autonomous substates, each following unique relaxation kinetics during annealing (Kawakami and Pikal 2005). This relaxation distribution is often expressed using an empirical Kohlrausch–Williams–Watts (KWW) equation (Eq. 14.3):

$$\phi_{\mathrm{KWW}}(t,T) = \exp\left[-\left(\frac{t}{\tau(T)}\right)^{\beta_K}\right] = 1 - \frac{\Delta H(t,T)}{\Delta H(\infty,T)}, \tag{14.3}$$

where $\phi_{\mathrm{KWW}}(t,T)$, τ, and β_K $(0 < \beta_K \leq 1)$ are the extent of relaxation, average relaxation time, and distribution parameter, respectively, at time t and temperature T. The narrower relaxation distribution of substates tends towards unity of β_K while β_K approaches to zero for higher dynamic heterogeneity. Here, $\Delta H\,(t,T)$ and $\Delta H\,(\infty,T)(= \Delta C_P\,(T_g – T))$ are the values of enthalpy recovery at annealing time "t" and that virtually at the completion of process, respectively. The KWW approach is limited to the systems with the relaxation times significantly larger than the annealing. A modified stretched exponent (MSE) function exists for the systems with very short ($t \ll T_1$) relaxation times with respect to the annealing times. DSC

is extensively used to study the effect of annealing to mimic the aging during storage of amorphous pharmaceuticals (Hancock and Shamblin 2001). DSC measures enthalpy recovery equivalent to the relaxation, provided the recovery is not accompanied by other physical or instrument-related factors. The recovered enthalpy at T_g is largely the consequence of α-relaxation. Precise integration of both the T_g and the superimposing enthalpy recovery measured by conventional DSC can be problematic. A direct correlation has been shown between the ratio of the height of recovery overshoot to ΔC_P and the β_K for some excipients (Pikal et al. 2004).

The fictive temperature (*temperature of the equilibrium supercooled liquid that is isoenthalpic to the glass*) progressively decreases towards the annealing temperature with time. This limits DSC annealing approach by the fact that relaxation time progressively increases while aging. Also, it is important to introduce the temperature correction for ΔC_P in view of the temperature dependence of the latter. The τ and β_K obtained by fitting KWW or MSE expressions are reported to be significantly higher and lower compared to their initial values, respectively. The annealing period greatly affect these values as well. The time constant, τ^{β_K}, has been found comparatively invariant to the annealing period and thus more reliable. Meaningful comparison of τ among systems requires similar β_K (Kawakami and Pikal 2005). Another concern is the possible overestimation due to extra annealing while heating at slow rate in mDSC. A frequency-related T_g shift in the RHF relative to the THF signal gives an endothermic signal in NRHF overlapping with enthalpy recovery. This effect can be subtracted from the actual signal by measuring the same in the cooling cycle in identical experimental condition (Kawakami and Pikal 2005). However, there would also be enthalpy loss while reaching to and mainly τ^{β_K} while residing at the annealing temperature. Therefore, it is advisable to correct the enthalpy recovery data by subtracting the signal obtained from frequency- and temperature-effect together from a time-zero sample.

There are fewer recent literature on the relationship of the ΔT_g and molecular mobility (Chieng et al. 2013a, b). As the increase in β_K tends the system to approach equilibrium faster, the larger β_K is associated with narrower ΔT_g. A study suggests that τ^{β_K} measured by mDSC for amorphous API, such as indomethacin and nifedipine, below T_g showed Arrhenius-type temperature dependence while that for ketoconazole showed typical VFT behavior (Bhugra et al. 2006). Caron et al. 2010 determined the value of τ^{β_K} for amorphous nifedipine and phenobarbital and their ASD in PVP by mDSC and found a correlation with sub-T_g crystallization. The relaxation time constant of indomethacin/PVP ASD obtained by mDSC is proposed to represent the bulk relaxation (Hasegawa et al. 2009). The different τ^{β_K} values of the differently prepared ASD of the same system indicate their diverse structural dynamics (Ke et al. 2012). The general utility of KWW to describe the molecular mobility of ASD is highly questionable unless the real chemical identities of the relaxing domains are known. The complex non-KWW behavior of enthalpy decay obtained by DSC has been reported for many ASD of wherein individual components show KWW profiles. For example, such observation for celecoxib/PVP has been attributed to their different composition-dependent H-bonding interactions (Bansal et al. 2010).

The enthalpy recovery in DSC of sub-T_g relaxations is often feeble and the relaxation time decreases upon annealing, and thus DSC is not sensitive enough to

probe the isolated local mobility (Bhattacharya and Suryanarayanan 2009). In general, the β-process contributes more at the lower annealing temperature/longer time in DSC. Therefore, the sub-T_g recovery temperature increases with longer time and/or higher temperature of annealing due to the increasing involvement of the α-process. Vyazovkin and Dranca (2006, 2007) have published their works on the use of DSC for studying β-relaxation of various organic glasses including that of some APIs and polymers. Amorphous PVP, indomethacin, and ursodeoxycholic acid annealed at various temperatures below $0.8T_g$ in DSC and the enthalpy recovery peaks during subsequent analysis were only observed for samples annealed at or above a certain temperature (Vyazovkin and Dranca 2006). Interestingly, activation energy for β-relaxation obtained from heating rate dependence of the recovery temperature showed satisfactory correlation with T_g for PVP and APIs. The sub-T_g peak of the β-relaxation of maltodextrin was observed to be influenced by temperature and humidity (Descamps et al. 2009). DSC sometimes provides indirect information on surface versus bulk relaxation behavior of ASD. Puri et al. (2012) annealed celecoxib/PVP/meglumine ASD with two different thicknesses and found that the enthalpy recovery for ASD with relatively higher surface-to-volume ratio was approximately three times higher compared to those for the ASD with lower values.

14.2.2 Molecular Miscibility and Compositional Homogeneity

DSC historically stands at the forefront for studying the molecular miscibility and phase homogeneity in ASD. Despite many limitations inherent to this technique, it is the first-line technique to screen the feasibility of molecular dispersion formation and to study solid-state miscibility in ASD before and during stability studies (Baird and Taylor 2012). Deconvolution of overlapping signals by mDSC facilitates phase analysis of ASD over conventional DSC. Fast scanning DSC can analyze the materials that are difficult to amorphicize (Guns et al. 2010). Depending upon the composition, a single mixed T_g (T_{gm}) of a miscible binary ASD can normally be distinguished from that of the API or the polymer. However, strong drug–polymer intermolecular interactions such as ionic/polyelectrolytic interactions, salt formation, or others can increase the T_{gm} to be higher than that of individual components (Weuts et al. 2005) as recently shown for a hydrogen bonding (H-bonding) system (Calahan et al. 2013). A single T_{gm} is considered as an indicator of complete molecular mixing between drug and polymer. For completely miscible compositions, volume additivity expressions of the Gordon–Taylor or Couchman–Karasz approach (Couchman and Karasz 1978; Gordon and Taylor 1952) aid the calculation of T_{gm} assuming the equivalent strength of homo- and heteromolecular interactions in the system. Therefore, positive deviation of the experimental T_g from the predicted one implies enthalpic contributions owing either to the strong intermolecular H-bonding (e.g., MK-0591/PVP) or to the negative excess volume of mixing (e.g., itraconazole/polyvinylpyrrolidone vinyl acetate, PVPVA; Kalogeras 2011), while negative deviations point to the predominant effect of positive excess free volume of mixing over

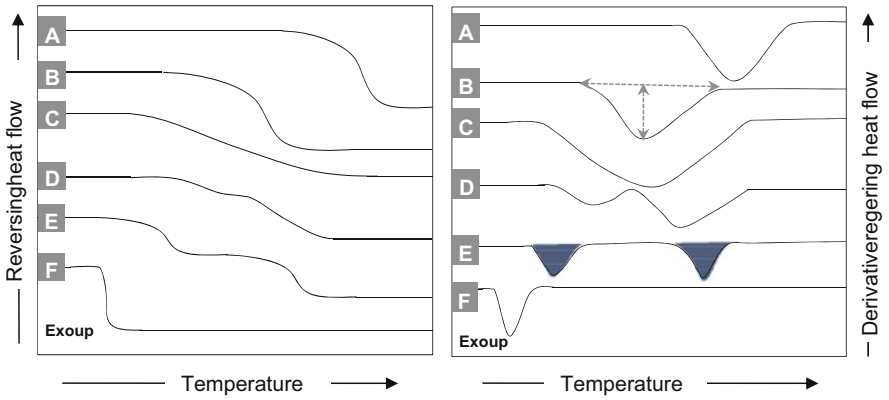

Fig. 14.2 An overlay of hypothetical mDSC thermograms depicting reversing heat flow (RHF; *left*) and derivate RHF (*right*) versus temperature. Trace *A*: polymer, *B–E*: various ASD, and *F*: API

either moderate-to-strong (e.g., felodipine ASD with PVP or hydroxypropyl methyl cellulose, HPMC) or weak-to-moderate (e.g., naproxen–PVP) heteromolecular interactions. Kalogeras (2011) modeled the experimental T_{gm} (composition) profiles of diverse ASD using an empirical expression. The H-bonding interaction has also been confirmed in a drug candidate/PVP ASD wherein the T_g measured by DSC overlapped with the predicted Gordon–Taylor profile. This suggests the need of cautious interpretation of such data from thermal analysis alone (Tobyn et al. 2009).

Hypothetical RHF signals and the corresponding first-derivative RHF signals with respect to temperature (dRHF) observable of ASD bearing diverse physical structures are illustrated in Fig. 14.2 (B–E). At least two thermal transitions are clearly exhibited in phase-separated ASD, each originating from one of the partially or completely separated phases. The separated phases rich in API and polymer exhibit respectively low and high T_g that are positioned distinctly apart provided sufficiently different composition (*E*). In such case, the ratio of ΔC_P of two phases or moreover the height or area of peaks in dRHF signals can be comparable with the phase composition (Paudel et al. 2013). On the other hand, when the composition of separated phases is not too different, borderline merger of two T_g's can be observed (*D*). For this, the corresponding dRHF signals can provide clearer identification. The lesser the difference between two T_g's, the more homogeneous the system is (Paudel and Van den Mooter 2012). Apart from the number and position of T_g, the shape of the transition can also provide information on the molecular state of ASD. For instance, the width and the symmetry of glass transition are very important features. Although the mid-positions of the glass transition seem similar for lines B and C, their shapes strikingly differ pointing the criticality of the shape/width in interpreting the compositional homogeneity. More precisely, the T_{gm} width of B is almost half that of C. As calorimetric techniques are reported to detect the phase separation into the larger domain size (> 30 nm), the wider T_g can be associated with heterogeneity possibly beyond the detection limit of DSC. The Raman chemical mapping has proven the

fact that a single T_g is not necessarily an indication of molecular miscibility (Qian et al. 2010). There is potential danger of introducing integration errors for feeble and wider signals to obtain the consistent T_{gm} midpoint and ΔC_P as of the case given in Fig. 14.2 (trace C). Rather, the use of the width and the area of the peak in the dRHF signal are seemingly reliable to describe the extent of microheterogeneties. Recently, increasing interests on the use of dRHF responses can be witnessed for polymer composites to model the blend homogeneity (Shi et al. 2013). The semiquantitative value of this simple data analysis approach has been applied for pharmaceutical ASD as well (Paudel et al. 2013).

The most problematic cases in distinguishing a single versus two amorphous phases are: ASD consisting of drug and carrier with essentially similar T_g's such as felodipine and Eudragit® EPO (T_g difference $< 3\,°C$; Qi et al. 2010a, b). Locating T_{gm}'s belonging to drug-rich and polymer-rich domains was found ambiguous for the phase-separated compositions of itraconazole/Eudragit E100 ASD (T_g difference $\leq 5\,°C$; Janssens et al. 2010). Instead, the respective enthalpy- recovery endotherms in NRHF signals facilitated the distinction of the T_{gm} positions. Enthalpy recovery can also be apparent even for a very small fraction of separated phases in NRHF traces that could otherwise not be contrasted from the RHF baseline. Sometimes, the presence of enthalpy recovery of the separated phases indirectly ensures that phase separation had occurred in the original sample rather than the in situ separation induced by heating in DSC. Analysis by fast scanning DSC can be superior as the decrease in the exposure time at higher temperature provides kinetically less-affected miscibility data. The inaccuracy often associated with C_P measurement of heterogeneous systems limits its routine use for studying the phase analysis of ASD. The change in phase angle, the angle between the modulated heating rate and modulated heat flow, can be correlated to phase separation through sophisticated deconvolution (Pieters et al. 2006). Such advanced mDSC experiments can worth the miscibility study of challenging systems. The DSC interpretation of ASD of API in multiple polymers needs further details. The mDSC analysis of felodipine ASD prepared in a blend of immiscible polymers viz., Eudragit EPO and PVPVA, suggested that the increase in drug loading leads to the higher fraction of drug in the polymer in which the drug has higher solid solubility (Yang et al. 2013). Likewise, thermal characterization of ASD containing an API dispersed in a copolymer is complicated if the amorphous drug has diverse miscibility in the constituting monomers as evidenced from the miconazole dispersion in Kollicoat IR (*poly (ethylene glycol-co-vinyl alcohol)*; Litvinov et al. 2012).

14.2.3 Crystallization, Melting, Crystallinity, and Mixing Interactions in ASD

The use of DSC for studying isothermal/non-isothermal crystallization is extensively reported (Baird and Taylor 2012; Svoboda and Málek 2011). Although not always

mutually exclusive, an entire crystallization process proceeds through an initial nucleation step followed by the growth of nuclei. A very small fraction of a sample mass actuates the nucleation process, often indistinguishable by DSC. The crystallization exotherm usually evolves at a temperature (T_C) following the T_g while heating an amorphous glass (Fig. 14.1) and it can appear while slowly cooling the melt as well. There are cases where the crystallization exotherm is detected before T_g during both scanning and isothermal measurements for physically unstable API. Crystallization from the cryomilled amorphous etravirine was detected at T_g −32 °C (Qi et al. 2010a, b). DSC studies have revealed the atypical bimodal crystallization of milled amorphous griseofulvin wherein the first exotherm occur prior to the T_g (Trasi and Byrn 2012; Trasi et al. 2010; Willart et al. 2012). Such behavior was also noticed for other milled amorphous form of felodipine, sulfamerazine, piroxicam, hydrochlorothiazide (Chattoraj et al. 2012). Interestingly, the first crystallization event originates from surface that is followed by bulk process beyond T_g. Highest surface crystal growth rates around T_g were confirmed for APIs exhibiting surface crystallization (Otte et al. 2012).

Experimental conditions such as thermal contact with the DSC pan, sample particle size, heating rate, etc. can markedly affect the crystallization enthalpy. The integrated area under a single and symmetrical crystallization exotherm can directly correlate to the crystallization enthalpy and the activation energy (Svoboda and Málek 2011). The activation energy of the non-isothermal crystallization (E_C) can be determined using the modified Kissinger method (Eq. 14.4) using the heating rate (β) dependence data of T_C from a series of DSC measurements:

$$\ln\left(\frac{\beta^n}{T_C^2}\right) = -\frac{mE_C}{RT_C} + \text{constant}. \tag{14.4}$$

Here, n is the order parameter and m is the dimensionality of growth. In mDSC analysis, the positive overall periodic minimum heating rate ensures proper deconvolution of crystallization exotherm. Grisedale et al. (2010) studied crystallization kinetics of amorphous salbutamol sulfate using mDSC and found that the spray-dried product had the higher T_C and E_C compared to that of the milled ones and for the latter these values increased with milling time.

The polymer in ASD significantly retards API crystallization such that T_c increases and H_F increases. For specifically interacting ASD of a drug candidate with PVPs, T_C was directly correlated with the T_g of the polymer (Khougaz and Clas 2000). The polymer can also selectively decelerate or inhibit surface crystallization. The presence of 20 % PVPVA in griseofulvin/PVPVA cryomilled ASD shifted the first T_C while this surface crystallization exotherm completely vanished upon increasing PVPVA (Chattoraj et al. 2012). While T_{gm} being unaltered, nifedipine/PVP ASD exhibited the particle-size-dependent crystallization exotherm with lower T_C for smaller particle fraction (Miyanishi et al. 2013).

The common method for modeling both isothermal and non-isothermal crystallization kinetics from amorphous solids is the Johnson–Mehl–Avrami -Kolmogorov

(JMAK) nucleation-growth model (Eq. 14.5; Weinberg et al. 1997):

$$\alpha_C = 1 - e^{[(K(t-t_{ind}))^m]}. \tag{14.5}$$

Here K is the nucleation rate constant, t_{ind} is nucleation induction period, and α_C is the crystallized fraction at time t. The values of K and m are obtained by regressing the experimental data using the double logarithmic linear form of Eq. 14.5. Originally derived for a homogeneous single component system, zero or constant nucleation rate in course of crystallization assumed by JMAK model can be an oversimplification of nucleation process for the process starting from ASD. Furthermore, this model is advocated to be inefficient in explaining crystal impingement at higher α_C (> 0.8; Sousa et al. 2010). The JMAK model is occasionally modified to account for the decrease in nucleation rate accompanied by the increase in the growth rate while crystallization progresses. Yang et al. (2010) proposed a better kinetic model (than JMAK) that considers nucleation rate to be inversely proportional to the crystallinity in order to study isothermal crystallization of etravirine–PVP ASD. Yoshihashi et al. (2006, 2010) studied isothermal crystallization of flurbiprofen, tolbutamide, and naproxen from ASD above T_{gm} using DSC. Their method typically involves heating the sample above T_m of API, cooling below T_{gm}, heating to the intended temperature, and keeping isothermal until the API crystallizes.

Non-isothermal DSC crystallization data can often enable the quantification of initial amorphicity. Assuming complete crystallization of the amorphous fraction present during DSC analysis, the degree of amorphicity is simply the ratio of area under the crystallization exotherm to that under the melting endotherm (Baird and Taylor 2012). These two events occurring at different temperature need correction for the temperature-dependent enthalpy. Equation 14.6 determines the initial crystallinity including the correction for the possible noncrystallizing fraction (α_{NC}; Grisedale et al. 2010):

$$Crystallinity = 1 - \left[\frac{\Delta H_C}{\Delta H_m - (T_m - T_C)\Delta C_P} \times \frac{1}{(1-\alpha_{NC})}\right]. \tag{14.6}$$

The α_{NC} can be estimated as the ratio of melting enthalpy obtained on (partial) crystallization of fully amorphous material (during DSC analysis) to that of the pure crystalline material of same form. For materials undergoing degradation during melting, ΔH_m and T_m can be replaced by ΔH_C and T_C obtained for fully amorphous material, respectively. In case of API in pure amorphous form or in ASD undergoing complete crystallization during DSC, the ratio of ΔC_P at T_g of partially crystalline material to that of completely amorphous material gives the degree of amorphicity while that of ΔH_C of partially crystalline material to that of completely amorphous material gives the degree of crystallinity in the sample (Aso et al. 2009). Apart from simple crystallization and melting, the possible occurrence of multiple polymorphic or liquid transitions during heating of amorphous API or ASD complicates the direct determination of crystallinity from DSC data (Janssens et al. 2010).

Occasionally, unintentional residues of submicron or bulk crystals dispersed within fresh ASD is encountered or partial crystallinity may develop during storage (Janssens and Van den Mooter 2009). The melting transition(s) of API appears in

the DSC thermogram of partially crystalline dispersion. However, multiple kinetic effects should be considered before thermodynamic interpretation. Below melting temperature of the drug, a fraction of crystals can dissolve in the matrix near and above the T_g or melting temperature of the polymer (Qi et al. 2010a, b). Also, the exothermic process of polymer dissolution in excessively molten API can affect the melting endotherm of API. The crystallinity estimated as the ratio of ΔH_m of the API in ASD to that in the corresponding physical blend can possibly correct these kinetic effects (Yang et al. 2010). The extent of crystallization in efavirenz/PVP ASD was computed as the ratio of melting enthalpy of the API in the ASD after time t to that after maximum crystallization of the same ASD. The complete crystallization may not necessarily occur as 40 % efavirenz crystallization was reported at plateau time (steady state) from PVP-based ASD.

There exist cases where a slow scanning mDSC thermogram discerns no melting for partially crystalline ASD (Bikiaris et al. 2005), as case of naproxen–PVP solid dispersions (Paudel and Van den Mooter 2012). Crystallites inhomogeneously dispersed in a polymeric matrix could experience different local compositions and hence variable local melting temperatures. This spans the overall melting event over a wide range. Fast scanning DSC can detect melting probably due to hindered drug–polymer dissolution kinetics and increased sensitivity. This also sacrifices the resolution among the multiple events and poses interruption from other kinetic signals retained such as desolvation. Disappearance/diminution of a drug melting endotherm can possibly attribute to the very fine crystallites distributed within ASD matrix. For the trace amount of nifedipine or griseofulvin embedded in PVP, crystallite size reduction to several nanometers resulted in more than 10 % drop in T_m (Liu et al. 2007). Also, the reduction in melting enthalpy of submicron or nano level crystallites in ASD results from the alteration of the bond energy of surface atoms of small crystals on the internal energy (Liang et al. 2002). In absence of melting, the crystallinity can be indirectly estimated by the C_P change at a temperature $> T_{gm}$ during a heat-cool-heat DSC method. The C_P at a temperature would be lesser in the first heating due to an initially present crystalline fraction as compared to that obtained during the following cooling or subsequent heating cycle. The heat-cool-heat mDSC program enabled the quantification of the API crystallinity of felodipine/Eudragit® EPO ASD (Qi et al. 2010a, b) and surface crystallinity of nifedipine–PVP ASD developed during aging, but with undetectable melting (Miyanishi et al. 2013).

Melting temperature of API in a solid dispersion obtained under quasi-equilibrium conditions also inherit a wealth of information about the drug–carrier mixing interaction (Sun et al. 2010). The overall chemical potential decreases when an API is dispersed in a polymer matrix leading to the depression in its equilibrium melting temperature. The depression is higher for stronger favorable (exothermic) interaction existing between mixing components. The composition–melting point profile for a drug/polymer system can yield the activity coefficient of molten drug in polymer, the Flory–Huggins interaction parameter and consequently the thermal phase diagram (composition-Gibbs free energy of mixing). These thermodynamic state functions are applicable at their best to the equilibrium data requiring the investigational system prepared with the least input of kinetic energy. DSC data of dispersions prepared

by slow solvent evaporation (Paudel et al. 2012) are closer to the assumption (Caron et al. 2011) than by spray drying or milling. Extrapolation of heating-rate-dependent melting temperatures to 0 °C/min heating rate yields quasi-equilibrium melting temperatures, which minimize the kinetic effect and are more reliable for theoretical use. The crossing point of the melting line with the T_{gm} line as the function of composition provides the predicted solid solubility of API in polymer, which still remains experimentally unverified for many drug–polymer systems. The extrapolated endset melting temperature in DSC ideally indicates the completion of melting and thus is meaningful for miscibility analysis (Marsac et al. 2006).

14.3 Isothermal Microcalorimetry (IMC) Studies of ASD

IMC, a complementary technique to DSC, is a versatile and sensitive tool for nonspecific thermal activity monitoring (TAM) of heat change occurring during any physical, chemical, or biological process (Ball and Maechling 2009). TAM possesses extreme sensitivity towards the heat flow (0.1 μW) and temperature change (10^{-4} °C), therefore suitable for quantitative analysis of several processes. The applicability of IMC has been extensively proven in monitoring subtle thermal events originating from processes such as mixing, chemical degradation, crystallization, and other phase transformations (Gaisford 2005). The TAM enables calorimetric experiments on various solid-state processes under controlled temperature and relative humidity (RH). The isothermal temperature is accurately maintained by a water bath surrounding a sample vial while a hygrostat containing saturated aqueous salt solution optionally placed along with a sample creates the designated RH at a set temperature (O'Neill and Gaisford 2011). The RH of the sample headspace can be continuously varied by passing the programmed composition of dry (0 %RH) and wet nitrogen (100 %RH) through a mass flowmeter. This RH perfusion microcalorimetry can probe various interactions through moisture-induced thermal activity traces (MITAT; Lechuga-Ballesteros et al. 2003). When operated as isothermal solution microcalorimetry (SC) or isothermal titration microcalorimetry (ITC), IMC measures solution or solution-mediated processes (Ehtezazi et al. 2000). The solid or liquid analyte is sealed in a glass vial (and equilibrated in a specific liquid) which can be broken to release the sample in the solution which results in the heat flow due to mixing and/or dissolution in SC while during an ITC experiment the heat flow generated from titration of continuously dispensed analyte in the liquid equilibrated inside the calorimeter is measured (Blandamer et al. 1998). A heat-conduction IMC measures heat flow (dq/dt) from ongoing processes in a sample. The detected electrical power (P) is the product of the voltage (U) generated by the temperature difference due to a thermal process in the sample and a calibration constant (ε_C). Generally, the exothermic process is represented by a positive signal and the endothermic event by negative signal in a heat flow curve. The integration of the heat flow curve (power data) over a particular time interval provides heat (q). Provided the total enthalpy of a

process (Q) is known, the temporal calorimetric data generates a solid-state kinetics in the form of a fraction converted ($\alpha = q/Q$; Sousa et al. 2010).

In spite of superior sensitivity, various challenges associated with IMC, e.g., larger sample size (50–200 mg) and limited temperature range (10–80 °C) restrict the types of experiments possible on amorphous samples. The thickness and sample amount play vital role on the eventual onset of surface versus bulk induction kinetics (Gaisford et al. 2009). The analysis time including the preceding equilibration is so long that the initial data points for fast processes such as the induction of enthalpy relaxation, nucleation/crystallization can escape detection. In contrary, ceaseless heat flow originating from some of very slow processes might not return to the baseline within the experimental period. Another main concern about IMC is the nonspecificity of the recorded TAM signal as the outcome of the entire processes taking place during the experimental period. This can hinder the data interpretation of amorphous systems possessing temporally overlapping processes such as relaxation, phase separation, and nucleation/crystal growth. For elevated static humidity or RH perfusion microcalorimetry, the potential degradation of labile components or moisture sorption/desorption/condensation signals can present further aberration in the measured data (Buckton and Darcy 1999). The optimal experimental conditions such as small sample size, temperature, gas flow rate, and RH ramp rate should be maintained to obtain (quasi)equilibrium measuring environment and an acceptable signal to noise ratio. Since thermal history of a sample cannot be erased prior to IMC analysis, it is extremely crucial to have consistency of process history, formulation conditions, and more importantly residual solvent of samples. At positive end, the feasibility of "*as is*" sample analysis by IMC can have discriminative advantage to detect the subtle structural change in ASD inherited from formulation and/or manufacturing processes (Kawakami and Pikal, 2005). Some existing applications of IMC relevant to amorphous pharmaceuticals are presented below.

14.3.1 Enthalpy Relaxation Studies on Amorphous Pharmaceuticals by IMC

The quantitative application of IMC for the rate of enthalpy relaxation of a pure amorphous APIs and excipients are explicitly documented but unfortunately few examples are available hitherto for ASD (Caron et al. 2010). Exothermic heat flow is detected in TAM below T_g as a consequence of relaxation. During IMC measurement, the early data points are often excluded during data analysis to avoid noise resulting from sample positioning (Kawakami and Pikal 2005). However, IMC records more temporal data points during enthalpy relaxation and hence yields relaxation parameters from a single run when compared to DSC. Thus, the power–time profiles obtained in TAM can be directly treated with the power equations of relaxation models viz., KWW (Eq. 14.3) or MSE equation with respect to time. The derivative form of the MSE equation can describe the experimental relaxation data measured by IMC more consistent, especially those recorded at lower annealing temperature (Kawakami and

Pikal 2005). The study of Bhugra et al. (2006) on diverse amorphous APIs revealed that the relaxation time constants measured below T_g by IMC for indomethacin and ketoconazole were notably shorter than those measured by mDSC. However, the extrapolation of the data trends measured by both techniques conversed at T_g.

The IMC relaxation data for ASD are complex to understand as well. Alem et al. (2010) investigated enthalpy relaxation of amorphous mixtures of sucrose–lactose and sucrose–indomethacin. For the mixture components with comparable relaxation times, physically meaningful relaxation parameters were obtained by modeling the experimental data of binary mixtures with the derivative KWW and MSE expressions. As the individual relaxation times differ markedly, the KWW relaxation parameters lost the ability to confer a physical meaning while MSE parameters were still meaningful. The relaxation time constants of nifedipine/PVP and phenobarbital/PVP ASD below T_{gm} using IMC data were significantly lower compared to those from mDSC (Caron et al. 2010). Moreover, the lower crystallization onsets predicted by relaxation data from IMC than the experimental value for ASD was anticipated to stem from the possibility of IMC measuring the α-process as well as some fast relaxation irrelevant to crystallization and not measured by mDSC. Overall, β-value obtained using IMC is found to be smaller than obtained using DSC data of amorphous API as well of ASD (Bhugra et al. 2006; Caron et al. 2010). The reason for the same is still controversial whether it is due to the higher portion of β-process measured by IMC or owing to the different impact of time-dependent molecular mobility in the two techniques. Chieng et al. (2013a, b) found that the relaxation times measured by IMC for ASD of starch derivatives and disaccharides and/or polyols to be directly proportional to one-third power of that derived from ΔT_{gm} methodology. Moisture-induced enthalpy relaxations are reported for amorphous sodium indomethacin sucrose, lactose, raffinose, and PVP using RH perfusion IMC (Lechuga–Ballesteros et al. 2003). The MITAT of amorphous spray-dried raffinose revealed an exotherm after a threshold RH originated from α-relaxation triggered by moisture (Miller and Lechuga-Ballesteros 2006). This was tested by recording MITAT at different RH scanning rate and by using samples with different thermal history. The relaxation exotherm expectedly vanished after *ex situ* annealing prior to analysis. Data on T_g–RH (moisture content) relation can assist the interpretation of MITAT.

14.3.2 Crystallization Kinetics of and Crystallinity in Amorphous Systems by IMC

IMC has been ubiquitously utilized for studying the isothermal crystallization kinetics of amorphous pharmaceuticals owing to the ultimate sensitivity of the technique towards subtle heat flow (Gaisford 2012). Low quantification and detection limit of the technique lead to enhanced crystallization enthalpy and therefore superior S/N ratio as compared to DSC. Several studies report the inert environment in studying crystallization kinetics or at static RH or scanning RH using RH perfusion calorimetry (Yonemochi et al. 1999). Different modified kinetic models are fitted to temporal data

on crystalline conversion to obtain crystallization parameters. For purely amorphous material undergoing complete crystalline conversion, the enthalpy of the crystallization exotherm from IMC equivalences the melting enthalpy obtained by subsequent DSC analysis (Buckton and Darcy 1999). The ratio of crystallization enthalpy of a partially crystalline sample to that of a completely amorphous reference provides the crystallinity. There are always chances to miss earlier induction points for rapidly crystallizing APIs especially in the absence of a crystallization inhibitor or while measuring at elevated RH. Sousa et al. (2010) estimated the total heat of crystallization by applying mathematical models on intermediate experimental IMC data points and found that the methods correctly predicted the heat of crystallization, in case of amorphous indomethacin. Thus, such models can enable the calculation of the total heat for missing data points of a very fast or slow process. The IMC study of Hédoux et al. (2009) on isothermal crystallization of amorphous cryomilled indomethacin exhibited an unusual broad exotherm with double peaks suggesting a possible overlap of a surface and bulk process. Interestingly, Bhugra et al. (2008) observed the early power curve essentially resembling the sub-T_g decay profile for amorphous indomethacin measured at $T_g + 20\,^{\circ}\mathrm{C}$ that was followed by a significantly longer nonzero baseline and a plateau before the crystallization exotherm. Since the expected relaxation time at this temperature ranges in ms–μs, the authors attribute the early decay to the decreasing nucleation rate triggered after the formation of stable nuclei population. The samples withdrawn from TAM before the exotherm and inspected by microscopy revealed that it already contained indomethacin crystals implying the lesser sensitivity of IMC for the crystallization induction. Crystallization studied using IMC of amorphous nifedipine after intensive mixing with glass beads showed markedly decrease of induction time in comparison to the untreated sample, the reason being the trace crystallinity developed during the longer mixing time (Song et al. 2005).

TAM signals recorded in humid condition must be interpreted cautiously. The crystallization enthalpy of lactose measured under elevated RH was markedly lower than the melting enthalpy by DSC (Hogan and Buckton 2001). Moisture triggers nucleation/crystallization beyond a critical RH by enhancing molecular mobility, often accompanied by desorption of water. The crystallization enthalpy obtained by IMC here (the exothermic heat of crystallization minus endothermic heat of desorption) would be lower than the melting enthalpy by DSC. The supply of the water of crystallization in RH perfusion calorimetry facilitates the hydrate crystallization of some materials that can restrain desorption. Crystallization enthalpy for the low mass of spray-dried amorphous raffinose recorded in TAM was equivalent to that of melting in DSC (Hogan and Buckton 2001). The sorption, evaporation, crystallization of salt, and sample wetting can contribute data recorded using aqueous salt solution hygrostat (Gaisford 2012). The additional plasticizer mixed with water is sometimes used to control headspace relative vapor pressure during TAM measurements. Yonemochi et al. (1999) studied isothermal crystallization of different amorphous ursodeoxycholic acid with the sample environment maintained using a varying ratio of ethanol–water. None of samples crystallized upon exposure to only humid air

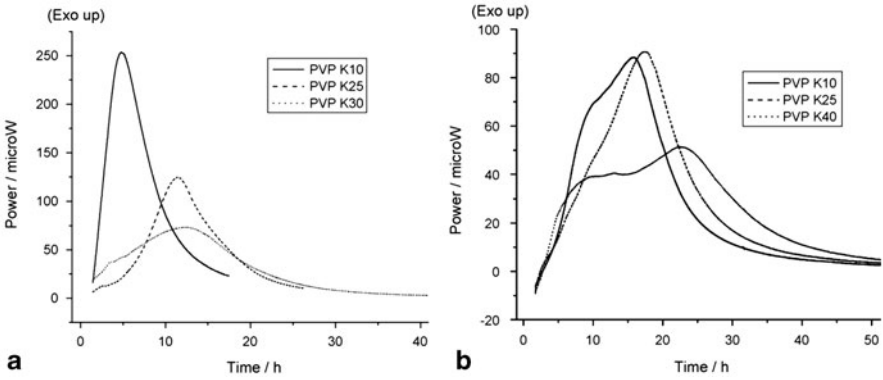

Fig. 14.3 Power–time data observed for indomethacin– PVP ASD films at 25 °C (**a**) and 37 °C (**b**). (Source: Gaisford et al. 2009, with permission from Elsevier)

while ground samples crystallized and quench-cooled samples did not crystallize in presence of ethanol vapor.

Although crystallization studies from ASD using IMC is challenging, Latsch et al. (2003, 2004) showed great potential of IMC in monitoring crystallization of amorphous steroidal drugs from dilute multicomponent transdermal patches. Transformation of amorphous estradiol dispersed in a matrix made up of acrylic polymer and polyethylene glycol (PEG) to hemihydrate was monitored using IMC (Latsch et al. 2004). Heat flow associated with drug crystallization expectedly increased with increase in drug loading in the formulation and was detected for drug loading even below 2 %w/w. In contrast to the case of amorphous indomethacin (Bhugra et al. 2008), the induction of estradiol crystallization from polymeric patches was detected quite earlier by IMC than by microscopy. Likewise, crystallization kinetics from a low amount of amorphous norethindrone acetate dispersed in a transdermal polymeric patch was studied using IMC (Latsch et al. 2003). The crystallization from the patch containing 4 %w/w drug was detected more by IMC than by microscopy. Crystallization from the patches with drug loading 4–10 %w/w was isokinetic while the rate was markedly accelerated from 12 % drug content. Crystallization kinetics from patches containing 2–14 %w/w mixtures of estradiol and norethindrone acetate dispersed in acrylic polymer and a plasticizer were studied using IMC (Latsch et al. 2004). The crystallization rate was the highest from patches containing PEG as a plasticizer. Gaisford et al. (2009) monitored the crystallization kinetics of indomethacin from ASD prepared with different PVP at 25 and 37 °C using IMC. As shown in Fig. 14.3, a crystallization exotherm was discernible at 25 °C while two adjoining peaks appeared at 37 °C. Post-TAM microscopy revealed that indomethacin entirely transformed into the stable γ-form at 25 °C while at 37 °C the early fraction (the first peak) transformed into the α-form and the second exotherm is attributed to the crystallization of the γ-form. No significant alteration in the overall crystallization profiles was apparent among the ASD containing different PVP. Urbanovici–Segal

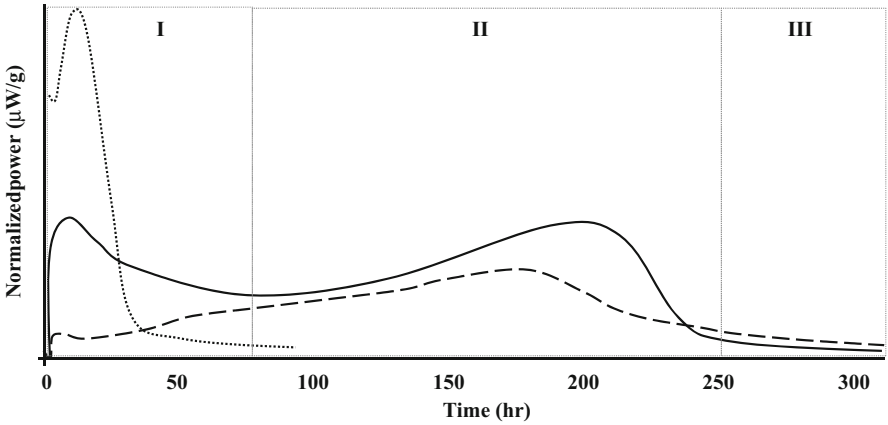

Fig. 14.4 TAM thermograms recording crystallization AMG 517 from pure amorphous state at 80 °C/25 %RH (. . .), from amorphous solid dispersions (ASD) with 50 %w/w hydroxypropyl methyl cellulose-acetate succinate (HPMC-AS) (- – -) and from ASD with 18 %w/w HPMC-AS (—). The region-I represents crystallization from drug-rich phase, region-II represents that from miscible ASD portion and region-III represents the absence of crystallization signal due to the amorphous fraction retained below solid solubility. (Adapted from Calahan et al. 2013)

models described experimental data better compared to the Avrami, Tobin model. Calahan et al. (2013) investigated the crystallization behavior of AMG 517, an investigational drug, from its ASD prepared in hydroxypropyl methyl cellulose-acetate succinate (HPMC-AS) using IMC at elevated temperature and RH. TAM thermograms (Fig. 14.4) exhibited the bimodal crystallization for ASD with higher drug load which turn into unimodal with decreasing drug content. The first exotherm of ASD overlapping the crystallization exotherm of the pure amorphous drug stems from the crystallization of amorphous drug clusters present in supersaturated ASD. The second exotherm originates from crystallization of drug from separated domains having miscible drug composition above the solid solubility while the remaining amorphous drug fraction is proposed to represent solid solubility of drug in the polymer.

IMC measurements under humid condition are also frequently used to quantify crystallinity in samples (Gaisford 2012). IMC is suitable for quantifying trace amorphicity (< 1 %w/w) in bulk crystals while the quantification of the trace crystallinity in bulk ASD is relatively inferior (Giron et al. 1997). The heat flow data are converted to initial amorphous content using the crystallization enthalpy or calibration curve. The contribution of unwanted processes while using saturated salt solution hygrostat, especially endothermic evaporation of water released during crystallization hinders quantification in small samples (Gaisford 2012). The RH perfusion cell overcomes many of these adverse effects. Addition of a drying (at 0 %RH) and a rewetting step after the crystallization step during the measurement is shown to provide the correction data for the wetting signal (Gaisford 2012). These methodologies are only valid in absence of all moisture-induced solid-state processes except crystallization, which is rarely possible for ASD. SC is an alternative technique for quantification of

amorphicity. The instantaneous heat flow signal from a solid in contact with a solvent constitute the disruption of solute–solute interactions (endothermic), solvent–solvent interactions (endothermic), and the solvent–solute interactions (exothermic; Van den Mooter 2012). The solute–solute interaction such as lattice energy significantly prevails in the crystalline substance over the amorphous from. Therefore, the dissolution enthalpy can be endothermic for a crystalline and exothermic for an amorphous form (Syll et al. 2012). Calibration curves in a suitable solvent can be used to quantify the amorphicity. Chadha et al. (2013) utilized SC to discriminate the structural features of amorphous hypoglycaemic agents prepared by different methods and to quantify the amorphous content in the sample. However, this methodology can again be limiting for ASD. The THF subsequent to the introduction of solid in a solvent will originate from different strength of drug–solvent, drug–carrier, and carrier–solvent interactions. Rather, this makes SC a useful technique to study the nature of interaction in binary systems and to estimate the heat of mixing between the dispersion components (Casarino et al. 1996).

14.4 Powder X-ray Diffractometry (pXRD) and X-ray Scattering

X-ray diffractometry (XRD) is a gold standard technique for studying crystalline materials. Several properties associated with long-range three-dimensional (3D) periodicity of crystals such as unit cell dimensions, lattice parameters, etc. are accessible from XRD data. The single crystal XRD involves the measurements on a precisely grown single crystal, with the incidence of X-rays on entire crystallographic planes through continuous rotation thus detecting a series of spots resulting from constructive interferences of the diffracted X-rays. The crystallographic interpretations of pharmaceuticals are detailed elsewhere (Ochsenbein and Schenk 2006). Also, the basic theories of X-ray diffraction and scattering are decipherable in several standard text books and are beyond the scope of this chapter. Most samples, often present in powder form, contain crystals of multiple orientations and the diffraction is detected as continuous Debye rings eventually resulting in powder patterns. XRD analysis of polycrystalline powders is called powder X-ray diffractometry (pXRD). Bragg's law of diffraction must be satisfied for the diffraction of incident X-ray onto a given crystallographic lattice plane through a constructive interference of coherently scattered waves that are "in-phase" in a certain direction (Eq. 14.7):

$$n\lambda = 2d \sin\theta \tag{14.7}$$

where n, λ, d, and θ are an integer (diffraction order), the incident X-ray wavelength, the spacing between a set of lattice planes, and the angle between the incident ray and the diffraction planes, respectively. Since d is a structural constant, either λ or θ needs to be varied to meet Bragg's criterion by all lattice planes present in a crystal. Most laboratory XRD measurements are carried out using a monochromatic X-ray source

by continuously increasing θ until the entire coverage of d and thus Bragg condition is met once at a time for each plane. The common sources with Cu and Mo produce X-rays with the wavelength of 1.5418 and 0.71073 Å, respectively. Another alternative is Laue diffraction wherein incidence of X-rays containing a range of wavelengths at fixed θ allows Bragg condition simultaneously for many planes as recorded by synchrotron X-ray source. High flux of X-rays from synchrotron source generates the supreme data quality, although the accessibility is limited and expensive. Common pXRD configurations are reflection and transmission mode. The Bragg–Brentano θ–2θ setup is the classical reflection geometry and the Debye–Scherrer geometry is a transmission setup. Transmission mode is suitable for low absorption samples and liquids, suspensions, etc. (in capillary sample holder).

The signals at a particular scattering vector, $Q\,(=4\pi \sin\theta/\lambda)$, represent the spatial density fluctuations in real space. Diffractometer configurations are common covering different ranges of scattering angle viz., $> 10°$ for wide angle X-ray scattering (WAXS) capturing structural information of < 1 nm, 0.1–10° for small-angle X-ray scattering (SAXS) and 0.001–0.3° for ultrasmall-angle X-ray scattering (USAXS; Dong and Boyd 2011). SAXS/USAXS are suitable for the analysis of liquid crystals, mesophases, macromolecules, dispersions, molecular self-assemblies, pores, colloidal structures, etc. (< 1–200 nm). The scattering measured in the Guinier's region by USAXS yields the radius of gyration of macromolecules. Simultaneous SAXS/WAXS instrument facilities provide in situ monitoring of *ms* scale phase transitions. Instruments measuring simultaneous SAXS/WAXS and DSC also exists (Pili et al. 2010). Some instrumental configuration selectively measures the surface scattering at the defined surface depth of the sample, e.g., grazing incidence measurements (Koch and Bras 2008).

A powder diffractogram is thus a plot of the diffraction intensity against 2θ or Q. The peak related to a particular space group is designated as a Bragg peak and is the signature of the crystalline material. The peak positions are related to the metrics of unit cell (d-spacing and other lattice parameters) and thus useful for qualitative phase analysis. The intensity and area under the Bragg peak are quantitatively associated with crystal structure (atomic positions, occupancy, etc.) while peak width to the crystal defects (strain, disorders) and size of discrete domain of crystallites. The Scherrer equation expresses the volume averaged thickness normal to the reflecting plane of crystallites with uniform size and shape as the reciprocal of full width at half height of the Bragg peak in radians (Patterson 1939). Background signals from the sample, holder, air, etc. and instrument-related broadness from polarization and optical shadow factors should be identified and removed (Bates 2011).

An amorphous material exhibits translational, orientational, and/or conformational periodicity only at short range (Bates et al. 2006). The pXRD pattern of an isotropic amorphous material appears as a continuous halo without distinct Bragg peaks. A partially crystalline material exhibits the Bragg peaks superimposed over the amorphous halo. The X-ray amorphous pattern portrays the mean response of the average local order of an ensemble of short-range orders each constituting local energy minima and contributing the coherent X-ray diffraction (Bates 2011). Alteration of local structure during T_g hardly respond in pXRD recorded with laboratory X-ray

source. Sometimes, the demarcation of short-range order and disorder is ambiguous, the end-ordered dimension (e.g., nanocrystallites) being the persistence of the unit cell characteristics. The domain size depends upon molecular size and the distance between the neighbors. The periodicity limited up to five basic units of atoms or molecules or unit cells in a sample leads to X-ray amorphous pattern which can be liquids, glasses, mesophases, nanocrystals (Bates et al. 2006). Each amorphous system exhibits unique peak maxima profiles of a halo and the area ratio of different halos, even unique to the preparation methods. Remarkable different pXRD halos of amorphous indomethacin prepared by melt quenching and by cryo-grinding has been reported (Karmwar et al. 2012). Although mechanistically unclear, the multiple glassy states of the same system with altered configurational entropies and microstructures correspond to different kinetic modifications. There are existing debates on such altered microstructures on amorphous states relating to polymorphism (Hancock et al. 2002). Water exists in at least three different X-ray amorphous forms differing in density and short-range H-bonding pattern (Winkel et al. 2009). Below some cases of the pXRD analysis of local structures, miscibility and crystallinity of amorphous pharmaceuticals are presented.

14.4.1 Local Structure of Amorphous Pharmaceuticals Using Total X-ray Scattering

The total scattering data refer to the collection of all coherent scattering measured over the entire Q-space treating Bragg and diffuse scattering with equivalent gravity (Billinge et al. 2010). It is the plot of total scattering structural function $S(Q)$, intensity normalized by incident flux per atom, versus Q. The X-ray counts divided by the scattering cross section of the sample yields the square of the atomic form factor, $f(Q)^2$. The weaker signals at higher Q get amplified with the small value of $f(Q)$ at higher Q eventually providing information even of the weaker signal. $S(Q)$ depends upon the magnitude of Q rather than on the direction for isotropic materials and is the sum of intra- and intermolecular scattering (Benmore et al. 2013). The pXRD data recorded in a shallow sample holder with low background or a capillary holder with larger step size and longer counting time are preferred.

Fourier transformation of $S(Q)$ profiles generates a real-space function $G(r)$ called the atomic pairwise distribution function (PDF) and is popular for the analysis of total scattering data (Billinge 2008, Farrow and Billinge 2009). The PDF profile ($G(r)$ vs. r) presents the probability of finding an atom at a distance r from any reference atom and the product of peak area and distance relates to the number of the particular atomic pairs distributed in real space. While low-r peaks (< 2.5 Å) correspond to intramolecular distances, the high-r signals to the overlap of intermolecular packing and thus sensitive to the short-range structures (Benmore et al. 2013). Radially averaged 3D structural information obtained from the PDF traces of pXRD data can serve as interatomic fingerprint. Radial distribution function and differential PDF provide further details of local order such as atomic coordination number, i.e., the

number of neighboring atoms for a reference atom at distance r (Benmore et al. 2013, Farrow and Billinge 2009). Limiting r-region to 20 Å of amorphous pharmaceuticals avoids fitting artifacts (Newman et al. 2008). The PDF amplitude of amorphous materials falls rapidly along r compared to crystals and the r leasing to the virtual loss of $G(r)$ oscillation yields the size of coherent domains (Atassi et al. 2010). Benmore et al. (2013) characterized amorphous APIs using synchrotron X-ray diffraction and spallation neutron diffraction. Structural information was lost after 5 Å of both glassy and crystalline carbamazepine. Miconazole nitrate and clotrimazole consist of the altered structural motifs in amorphous states from the respective crystals while amorphous cinnarizine retains the crystalline conformational residue. The PDF traces suggested the weaker memory of γ-form present in the amorphous indomethacin prepared from both $\alpha$and γ forms (Bates et al. 2006). Multivariate analysis (MVA)-PDF can efficiently assess the degree and the nature of disorder during milling, storage time/temperature-mediated crystallization of milled amorphous material (Bøtker et al. 2011; Naelapää et al. 2012; Boetker et al. 2012). The rapid acquisition PDF using synchrotron radiation of Ca-ketoprofen uniquely discriminated amorphous and mesomorphous structures of the crystalline phase (Atassi et al. 2010). Total diffraction data of a drug candidate, GNE068, were used for the in-depth investigation of the disordered mesophase (Chakravarty et al. 2013).

One hurdle associated with meaningful PDF analysis is the need of the broad Q range. Evidently, liming the range of Q causes poor resolution and thus remarkable loss of structural information. Indeed, a synchrotron source is preferable to generate total scattering data with the highest resolution consisting of minimal statistical uncertainties. The PDF data with $Q_{max} < 18$ Å^{-1} constitute all structural features for pharmaceuticals (Atassi et al. 2010). Dykhne et al. (2011) found that the PDF fingerprint of amorphous carbamazepine is unambiguously correlated with that of crystalline form when recorded using synchrotron radiation ($Q_{max} = 20$ Å^{-1}), silver-anode ($Q_{max} = 15.9$ Å^{-1}) or molybdenum-anode ($Q_{max} = 12.5$ Å^{-1}) while statistically poor and suboptimal resolution was obtained with Cu-anode ($Q_{max} \leq 8$ Å^{-1}). The PDF of melt-quenched carbamazepine collected using a synchrotron source by Billinge et al. (2010) revealed the same to be nanocrystallites instead of being amorphous. PDF analysis of synchrotron data of amorphous indomethacin showed poor correlation with both crystal (Billinge 2008) that was apparent using a Cu source (Bates et al. 2006). Overall, discriminatory PDF analysis requires at least the data collected using a molybdenum source.

14.4.2 Molecular Miscibility in ASD Using pXRD and Computational Analysis

Traditional pXRD analysis ascertains amorphicity through the absence of Bragg peaks. As such, X-ray halo patterns of amorphous composites lack direct information on the miscibility compared to thermal methods. Various computational, chemometric, and statistical analysis treatments of the measured pXRD infer the qualitative and

semiquantitative information on miscibility in ASD (Ivanisevic 2010). Figure 14.5 depicts the general approaches for the miscibility assessment.

Since an amorphous physical mixture can be considered as the representation of the immiscible state, the pXRD of ASD overlaying a physical mixture implies amorphous immiscibility and any mismatch indicates miscibility. However, the miscibility inferred from this comparison is susceptible to the physical mixture preparation and many other factors. Provided the availability of reproducible X-ray amorphous halo of pure drug and polymer, it is convenient to generate pXRD pattern by linearly combining the weighted powder patterns of individual components (Fig. 14.5I). This digital pXRD pattern serves as the data for virtual physical mixture (Bates 2011). The change in local drug–drug and polymer–polymer coordination occurs in miscible ASD. Measurement under inert environment and low background improve the data quality for modeling (Newman et al. 2008; Ivanisevic et al. 2009). Since proper normalization of pXRD data is necessary before generating the digital pXRD, the type of normalization scheme can also affect ultimate results (Newman et al. 2008).

Likewise, the dissimilarity between calculated PDF traces from pure components and PDF trace of ASD qualitatively infer the miscibility. PDF transformation autonormalize data in an absolute scale of electron units amplifying subtle differences that enables robust fitting. If the ratio of the scale factors conversing the simulated PDF pattern to the measured PDF of ASD results the theoretical drug/polymer ratio, the ASD is phase separated, otherwise miscible. Newman et al. (2008) contrasted the total percentage from composition calculated using PDF against the real composition for ASD of dextran–PVP, indomethacin–PVP, and trehalose–dextran dispersions. In agreement with T_g's of dextran and PVP exhibited by the DSC thermograms of ASD, the theoretical blend compositions could be correctly modeled by PDF. Higher deviation of PDF-derived total percentage from the true value is noticeable for the single T_{gm} indomethacin–PVP systems. However, the PDF data evidenced phase separation in dextran–trehalose ASD despite a single T_{gm}. Thus, PDF analysis detects phase separation in ASD with multiple T_{gm} as well as in the single T_{gm} system. Since PDF analysis experiences higher random errors compared to direct pXRD pattern analysis, statistical significance of the differences should be confirmed. Moore et al. (2010) utilized the error propagation in PDF analysis of miscibility. The sum of squares of the errors of the individual curves estimates the error in the difference between the measured and the digital PDF of ASD ($\Delta G(r)$ residuals). The statistical significance of the immiscibility/miscibility can be established through hypothesis testing. The inclusion of zero by the plot of $\pm 3\sigma$ interval around the residual plot throughout the r-range ensures the acceptable condition for inferring the immiscibility, e.g., terfenadine–PVP (Fig. 14.5III). While the exclusion of zero by the $\pm 3\sigma$ difference plot intervals indicates statistically significant dissimilarities between experimental PDF of ASD and the physical mixture indicating miscibility, e.g., felodipine–PVPVA 64 ASD.

Ivanisevic et al. (2009) applied pure curve resolution method (PCRM) and alternative least square (ALS) method to pXRD data of ASD for miscibility studies. The PCRM-based approach follows the analysis of the variance among the measured intensity points of pXRD patterns of ASD with varying drug loadings thus

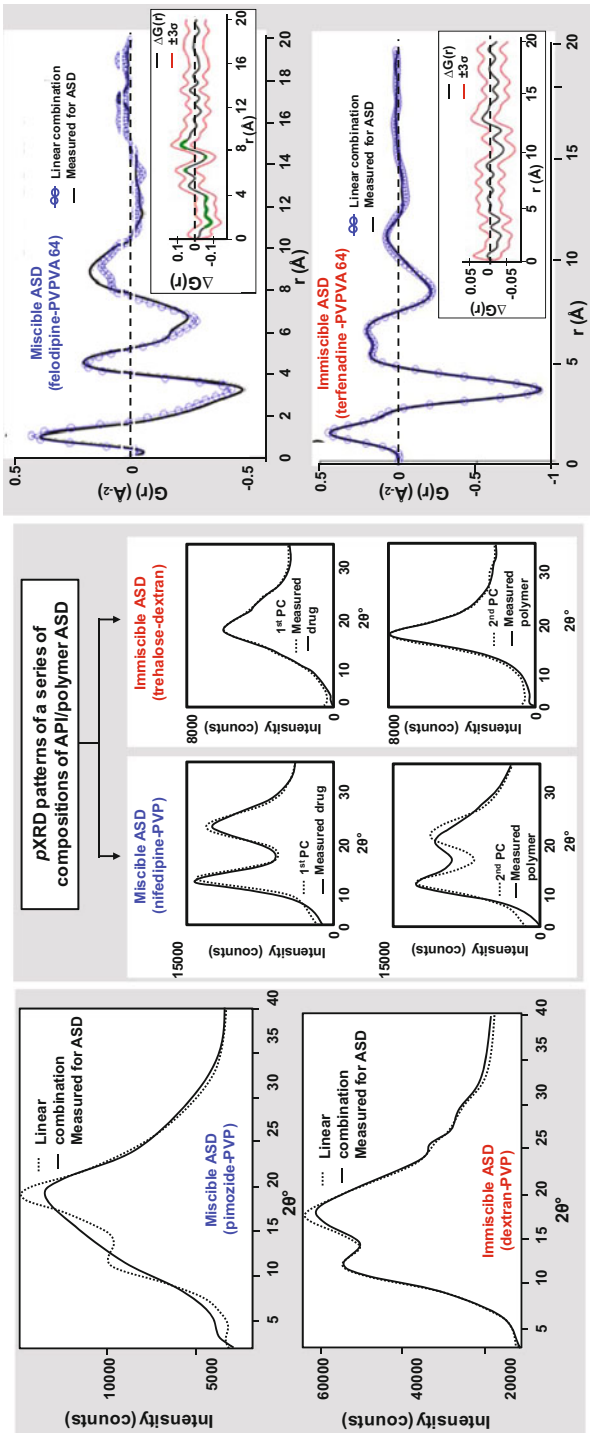

Fig. 14.5 Illustrations of miscibility assessment using powder X-ray diffractometry (*pXRD*) data: I. comparison of linear combination of drug and polymer pXRD patterns with measured pattern of *ASD*, II. comparison of pure component pXRD pattern extracted from multivariate curve resolution of ASD patterns with the measured patterns of pure components, and III. comparison of linear combination of drug and polymer pairwise distribution function (*PDF*) patterns with the PDF pattern derived from the measured pXRD data of ASD (residual plot with standard deviation is shown in inset). (Schemes are constructed based on Bates 2011; Ivanisevic et al. 2009; Moore and Wildfong 2011)

eventually allowing the extraction of pure curves (PCs), i.e., pXRD patterns of the constituting components (Fig. 14.5II). The variance of the measured powder patterns is describable by two extracted PCs representative of API and excipient for phase-separated systems representing the weighted drug–drug and polymer–polymer intermolecular interactions as per blend composition. The miscibility is diagnosed by the poor fit of extracted PCs with the measured powder patterns of pure components as drug–polymer coordination additionally contributes the orthogonal PCs of API and polymer (Fig. 14.5II, left panel). Additional component or the shift of the amorphous halo position(s) on the order $\geq 1°2\theta$ in extracted PCs can even indirectly indicate miscibility. The ratio of scale factors of PCs corresponds to the blend phase-separated composition. ALS approach can estimate the drug–polymer coordination number representing the degree of miscibility as the drug–polymer coordination substitutes the drug–drug and polymer–polymer coordination as a function of composition.

The homogeneity in ASD can be investigated within the range of 1–100 nm using SAXS (Laitinen 2009). The intensity and angular distribution of the scattered intensity in SAXS patterns can yield the size or surface area per unit volume of a constituting domain. Apart from the atomic structure, the electronic density variations of amorphous composites stem from the heterogeneity of the microstructure. Laitinen et al. (2009) studied the distribution of perphenazine in its ASD with PVP and PEG. The pair density distribution profiles as a function of cluster radius were extracted from SAXS data. The ASD exhibited a peak with maxima < 30 nm along with a minor peak at 70–90 nm, as for pure polymers. This was considered as the sign of molecular level dispersion formation. A subsequent SAXS study of the effect of storage at elevated humidity showed unaltered size of clusters pointing to the retention of molecular miscibility (Laitinen et al. 2010).

14.4.3 Crystallization Studies and Crystallinity of Amorphous Systems Using pXRD

The inherent specificity and quantitative power towards the crystalline state make pXRD as the technique of choice for studying crystallization from amorphous systems (Ochsenbein and Schenk 2006). Also, the instrumental flexibility allows in situ monitoring of crystallization as function of time, temperature, pressure, RH, or combinations. An API can crystallize to different polymorphs from ASD (Guns et al. 2011). The reference powder pattern enables the identification/quantification of the polymorphs developing in ASD (Ivanisevic et al. 2010). Preferred orientation of crystalline faces is a major source of error. Generally, analysis in transmission mode reduces the preferred orientation and avoid other instrumentally induced distortions and anisotropic shifts (Moore et al. 2009).

Quantification of the degree of crystallinity present initially, induced during storage or processing in amorphous pharmaceuticals by pXRD is well established. The powder pattern of a partially crystalline dispersion includes Bragg peaks associated with the prominent crystal faces superimposed to the amorphous halo. The intensity

and area of Bragg peaks systematically increase with increases in crystallinity and in expense of the amorphous halo. An indirect quantitative method for crystallinity utilizes the ratio of intensity of Bragg peaks of the sample to that of the (internal/external) reference standard. Since the predominant amorphous fraction largely contribute to the diffraction pattern of ASD, an indirect method presents a major analytical challenge. The ratio of net areas of all Bragg peaks to the sum of areas of Bragg peaks and of the corresponding amorphous halos beneath at the respective 2θ obtained from the normalized pattern directly yield the degree of crystallinity in a sample (Paudel et al. 2013; Rumondor and Taylor 2010; and Zidan et al. 2012). This is a common method for solid dispersions and works well unless the powder pattern comprises many overlapping peaks. Constructing calibration curves of partially crystalline dispersion is tedious for this approach since it is hard to generate the calibrants with identical microstructures as that of the analyte. Preferably, calibrants must contain ASD mixed with the known quantity of crystalline API. Modern pXRD software allows integrating the area under a particular Bragg peak and amorphous halo below it separately. Rumondor and Taylor (2010) found for felodipine–PVP system that the predicted crystallinity by partial least-squares (PLS) method exhibited less error compared to the area ratio method. The use of intensity ratio of a peak or a subset of characteristic peaks is also ubiquitous in quantifying crystallinity in ASD (Paudel and Van den Mooter 2012; Paudel et al. 2013). It requires all measurements under identical conditions and no peak broadening due to lattice strain or particle size and the use of an internal standard. If an ample region in pXRD pattern lacks Bragg peaks, the diffraction intensities of the noncrystalline regions representing the short-range order can be used to estimate the amorphicity (Ivanisevic et al. 2010). The difference in X-ray absorption coefficients of API and polymer should be duly considered before the quantitative analysis by such approach (Madsen et al. 2011).

More challenging is to quantify trace (nano) crystallinity in ASD. The Scherrer broadening due to the small and imperfect crystallites present in a low volume fraction can possibly bring the diffracted Bragg intensity down to that of the diffuse halo of an amorphous fraction (Koch and Bras 2008). These scenarios can lead to the false impression of complete amorphicity. Total scattering pattern enables quantification of trace crystallinity, since the scattering vector (Q) is proportional to the crystalline fraction (Liu et al. 2012). Benmore et al. 2013 quantified the trace crystallinity in various amorphous APIs by comparing the Bragg scattering intensity to the diffuse scattering intensity measured using synchrotron X-ray source. The intensities of the halo of various ASDs are shown to alter with aging as for PVP-based dispersions of nifedipine, felodipine, indomethacin, etc. (Ivanisevic 2010).

Temporal pXRD measurements enable monitoring in situ isothermal crystallization kinetics from ASD (Ivanisevic et al. 2010). Relative crystallinity is often estimated using the area ratio method at different time periods. The crystallinity degree at each time point is normalized with that at the point where crystallization reaches a maximum and is stationary. The extents of crystallization can be plotted as a function of time and modeled using diverse models of crystallization. Since the fractals and particulate properties of growing virgin crystals are difficult to predict, only relative crystallinity can be estimated with such experiments and is sufficient for

comparison of kinetics. Also, long pXRD-recording programs may enhance crystallization rate by X-ray energy leading to the overestimation of the rate as reported for APIs like nifedipine (Ivanisevic 2010). Paudel et al. (2013) monitored the kinetics of crystallization of naproxen at 94 %RH from naproxen–PVP ASD prepared by spray drying at various process parameters.

14.5 Gravimetric Vapor Sorption (GVS)

The moisture–solid interaction is an inevitable aspect of pharmaceutical development. Elucidation of moisture-induced physical alterations in amorphous pharmaceuticals is crucial, especially for ASD. Gravimetric measurement on the rate and extent of moisture gain (sorption) by or loss (desorption) from amorphous samples as a function of RH or as a function of time at a constant RH (isohumic condition) can provide a wealth of information of ASD. The key structural properties of ASD measureable by moisture sorption/desorption are drug–polymer interactions, moisture-induced glass transition, crystallization, hydrate formation/dehydration, etc. while that associated with particulate or bulk properties are hygroscopicity, diffusivity, pore size, surface area, etc. (Burnett et al. 2009).

The traditional way of installing the desired RH is by using a saturated aqueous solution of a particular salt or salt mixture (Greenspan 1977). Commercial instruments are now available, which can measure gravimetric moisture sorption and desorption while applying an RH ramp or at the selected humidity, known as dynamic or gravimetric vapor sorption analyzers (DVS or GVS; Penner 2013). Thus, moisture sorption/desorption isotherms can be expressed as a function of RH or time. The sorption isotherms may appear in various shapes for different types of samples and several theoretical models exist for describing different types of sorption isotherms, which is beyond the scope of our current discussion. The interested readers are referred to the standard books for the details (Reutzel-Edens and Newman 2006). In addition, moisture diffusivity in an amorphous solid matrix is an extremely complex process, which depends upon the hygroscopicity, texture, microstructure, porosity, surface chemistry and particle size, morphology, moisture-induced structural relaxation and phase transformations as well as the extent of water content. Different models have been proposed to account these phenomena, but none can provide complete account of all underlying processes (Perdana et al. 2014).

An interesting use of GVS, for amorphous dispersions, is detection and quantification of crystallinity. Due to higher hygroscopicity of hydrophilic polymers and amorphous API of ASD, the exposure of a sample to elevated humidity environment triggers the sorption of water molecules by polar/hydrophilic functional groups at the air–solid interface. The α-relaxation time of amorphous material often correlates with its water sorption potential (Bhardwaj and Suryanarayanan 2013). The gravimetric vapor sorption (GVS)–desorption led to the dissimilar structurally reversal of annealed amorphous trehalose when compared to that obtained by heating beyond T_g (Saxena et al. 2013). The sorbed water molecules ($T_g = -137\,^{\circ}\mathrm{C}$) increases

the molecular mobility and plasticize ASD (Rumondor et al. 2009). The extent of depression of T_g due to moisture sorption depends upon the water—sample intermolecular interactions (Yuan et al. 2011; Crowley and Zografi 2002; Roos 1995). The moisture-induced glass-to-rubber transition drastically increases sample fluidity after a certain RH. With sufficient moisture sorption and time, the increase in molecular mobility facilitates the energy barrier and hence induces nucleation/crystallization. Crystallization of an amorphous phase sharply reduces the tendency of moisture sorption and this might be apparent from the change in the slope of the sorption isotherm from the particular RH (Hancock and Dalton 1999; Roe and Labuza 2005). The moisture-induced nucleation and crystal growth manifest drastic reduction in surface area (voids/spaces) and surface free energy of the sample. This appears as a sharp drop in the moisture sorption profile originating from the loss of excess water during crystallization. The plots of extent of mass loss as a function of time yield the crystallization kinetics profile at particular RH. Temperature also imparts the synergistic effect on the induction point (RH or time) of crystallization. The ratio of moisture induced reduced T_g to the onset of crystallization for amorphous lamotrigine mesylate was fairly constant over a wide range of RH and temperature combination (Schmitt et al. 1996). Interestingly, the logarithm of onset of crystallization time below T_{gm} (dry) was linearly related to the ratio of reduced T_{gm} to the experimental temperature (corresponding to the combination of RH/T) for ASD of the drug candidate SAR and HPMC phthalate (Greco et al. 2012). Yang et al. (2010) reported the linear relationship between the crystallization constant and RH for efavirenz–PVP ASD. Various methods have been reported for the quantification of amorphous content below 1 % using GVS that are based on the inherently higher hygroscopicity of amorphous phases compared to crystalline counterparts (Young et al. 2007). The extent of equilibrium moisture sorption at a particular RH for calibrants with known amorphicity enables the quantification. However, the possible contribution of various accompanying phenomena, such as moisture-induced phase separation, limits the quantitative application of GVS at higher amorphous content. Another hurdle in using GVS analysis for the precise quantification of crystallinity of an API in pure form or in ASD would be for the system wherein the incomplete crystallization occurs even by the end of the DVS cycle, which indeed implies the reliance on the complementary confirmation data post DVS analysis (Qi et al. 2010a, b).

Gravimetric moisture sorption data at a particular RH provide an estimate of the strength of binary intermolecular interactions among drug, polymer, and water molecules and hence the extent of moisture-induced destabilization possible in ASD (Crowley and Zografi 2002; Paudel et al. 2010). By applying Flory–Huggins–Vrentas expressions for drug–polymer–water systems, drug–polymer interaction parameters have been derived from the moisture sorption data of physical mixtures or ASD of many drug–polymer systems (Paudel et al. 2010; Rumondor et al. 2009). The non-covalent interactions such as H-bonding established by hydrophobic drug with the hydrophilic moiety of the hygroscopic polymer in ASD lead to the reduction of moisture sorption by the polymer in ASD compared to the pure state, the process

sometimes known as hydrophobization. Therefore, stronger drug–polymer interactions makes the polymer more hydrophobized and hence leads to the larger negative deviation of moisture uptake by ASD as compared to the linear addition of weighted values for drug and polymer. The PVP/VA 64-Eudragit ASD markedly retarded extent and rate of water sorption compared to the corresponding physical mixture (Yang et al. 2013). The same polymer blend loaded with 10 % felodipine prepared by melt extrusion showed drastic improvement on the moisture protection for the amorphous system. With some geometric assumption, van Drooge et al. 2006 utilized a model to estimate the size of amorphous diazepam clusters dispersed in phase-separated PVP-based ASD using moisture sorption data. The thickness of the hydrophobized layer and volume of hydrophobized PVP were estimated assuming that the drug dispersed at molecular level reduces the hygroscopicity more than clusters having less drug–PVP contacts. The estimated size of amorphous drug clusters increased from 9.6 (265 molecules) to 20.8 nm (2674 molecules) while increasing the API content from 35 to 65 % in phase-separated ASD.

14.6 Other Techniques

Besides thermal, diffractometric, and moisture sorption techniques, there are ample other techniques, as aforementioned, that are commonplace for the analysis of the various structural features of ASD. Table 14.1 lists various techniques and brief descriptions for their measuring principles relevant to ASD. The details of working principle and various other applications of these techniques are available elsewhere. Some representative and relevant references are also included in Table 14.1. Tables 14.2–14.8 portray the structural characteristics measurable by various these techniques and also possible hurdles and interferences.

14.7 Regulatory Perspective of ASD Analysis

Chemistry, manufacturing and control of API, and dosage forms are strictly regulated by United States Food and Drug Administration (FDA; USFDA 2012). The current regulatory initiation towards the risk-based quality by design (QbD) approach encourages the implementation of a range of analytical tools varying in the depth of information, operational cost and time during different developmental stages and product life cycle (ICHQ8(R2) 2009). Many regulatory challenges thus apply on the analytical techniques characterizing and controlling the key quality attributes of these products. The inevitable qualities in any finished dosage form are the intended level of pharmaceutical performance and physical/chemical stability. Various molecular properties of intermediate and final product such as phase homogeneity, molecular mobility, miscibility, hygroscopicity, crystallinity, surface chemistry, etc. can principally govern the quality attributes of ASD-based products (in vitro dissolution,

in vivo behavior, and physical stability). Thus, characterization and monitoring of these physical attributes during preformulation, manufacturing, product release, and stability studies enable the priori control on the ASD-based product quality ensuring the patients need and the expectations of regulatory agencies. This requires various analytical techniques that interface among physical chemistry, materials science, surface chemistry, etc.

Preformulation studies furnish the physicochemical data including relevant solid-state properties (amorphous stability, crystallization kinetics, hygroscopicity, etc.) of a drug candidate intended for ASD development (biopharmaceutics classification system (BCS) II/IV) during preclinical stage. Early screening for polymer(s), (optional) surfactant selection and drug loading includes high-throughput solvent casting or melt quenching with a series of compositions (Paudel et al. 2012). At this stage, rapid and in situ analysis by polarized light microscopy and vibrational spectroscopic probes (IR, Raman) enable identification of the crystallizing systems and compositions. Furthermore, DSC analysis will assist for miscibility studies and composition-phase analysis. *In sample,* micro-dissolution follows the solid-state analysis that evaluates the stability of aqueous supersaturation generated by ASD (Wyttenbach et al. 2013). Again, spectroscopic probe or microscopy can monitor the physical manifestation, especially nucleation/crystallization or phase separation while in contact with the aqueous medium. Accelerated stability studies under the elevated RH/temperature can be studied in situ using pXRD or spectroscopy. These preclinical formulation prototyping supported by promising animal exposure data assist the nomination of first-in-human ASD and together constitute the data for investigational new drug submission.

More detailed product characterization increasingly stipulates sophisticated analytical tools while the clinical studies on drug candidate progresses. The physicochemistry of drug candidate and excipient(s) of the elected formulation and characterization data obtained during preclinical stage will guide the manufacturing feasibility studies at the laboratory scale and process selection for intermediate ASD during phase I studies. Implementation of various non-destructive spectroscopic process analytical technology (PAT) probes such as Fourier transform infrared spectroscopy (FTIR), Raman, near-infrared spectroscopy (NIR), or terahertz (THz) fiber optics at multiple locations of processing equipment will provide real-time monitoring of amorphization and evolution of desired physical properties such as compositional homogeneity or stabilizing interactions in the resulting ASD. This *in-process* supervisory control of product quality attributes will ensure running of the process within the design space. Such PAT tools have been successfully applied to some ASD manufacturing by hot melt extrusion (Saerens et al. 2013a, b). Analytical tools highly sensitive to the minute alteration in product physical structure can only discriminate the process parameters effect on physical attributes of ASD relevant to the performance and physical stability. Comprehensive studies on solid-state solubility and kinetic miscibility of the selected drug–polymer combination require mDSC experiments and spectroscopic studies. Thermoanalytical data can be modeled using suitable theoretical models to extract physical stability descriptors such as heteromolecular interaction parameters. Furthermore, vibrational spectroscopy

such as FTIR, NIR, Raman, and THz will help in identifying different stabilizing intermolecular interactions such as H-bonding. Often, these techniques can be insensitive to the subtle process-related microstructural variations. Therefore, use of total scattering (PDF) pXRD and SS-NMR spectroscopy/relaxometry is encouraged at this stage for the estimation of miscibility at molecular level. AFM-based techniques implemented to characterize molecular miscibility and stability of melt-quenched films has shown promising correlation to that obtained in the dispersion prepared by hot melt extrusion (Lauer et al. 2013). SS-NMR or sensitive pXRD measurements can verify various features such as the extent of molecular interaction, crystallinity, domain size, etc. achievable by faster techniques such as NIR, Raman. Detailed elucidation of various kinetic processes concomitantly occurring during bio-relevant in vitro drug dissolution such as nucleation/crystallization, plasticization, polymer swelling, aggregation, etc. can facilitate more rational correlation with in vivo human pharmacokinetic data. Various spectroscopy probes (IR, Raman, THz), microspectroscopic imaging (NIR, Raman, MRI, etc.), microscopy to scattering techniques (SAXS and SANS) can provide different level of information in such investigations.

Rigorous dosage from development and manufacturing activities commencing parallel to the phase II clinical studies further commend stronger analytical support. DVS moisture sorption/desorption analysis, surface analysis using time-of-flight secondary ion mass spectroscopy (TOF-SIMS), X-ray photoelectron spectroscopy (XPS), IGC, or localized thermal analysis will help in the process-related effect on the surface versus bulk microstructure of ASD that can be relevant to physical and chemical stability. Comprehensive elucidation of primary and various secondary molecular motions using DES, thermally stimulated discharge current (TSDC), or SS-NMR can help in predicting the physical stability against crystallization. The projected stability under stressed condition can be experimentally verified. Advanced multidimensional SS-NMR spectroscopy/relaxometry will provide the superior dynamic and structural information of ASD product that can be correlated with the process as well as performance. The intended products of most ASD are solid oral dosage forms such as tablets and capsules. This necessitates various particulate level characterizations (powder flow, micromeritics, etc.) as well as compatibility studies of API in ASD in presence of the intended adjuvants such as fillers, binders, lubricants, etc. With the further dilution of drug in the finished product, the analytical tool needs to more sensitive. The use of localized tests with spatiochemical specificity such as microspectroscopic imaging (NIR, Raman) and micro/nano-thermal analysis can be more helpful in elucidating content as well as phase distribution. Further, sound understanding on the effect of downstream processing such as granulation, compaction, coating, etc. on the product microstructure require surface sensitive and discriminatory techniques. Compression can also lead to molecular demixing in some systems (Ayenew et al. 2012). Dynamic TOF-SIMS revealed the orientation of pyrrolidone group of PVP towards the surface during compression to develop tablets containing PVP-based ASD (Leane et al. 2013). Coating-induced trace crystallization was detected by pXRD.

The commercial drug product manufacturing process with real-time monitoring is established by phase III clinical stage, since the intended commercial formulation

is preferably used for these studies. Therefore, robust PAT tools and well-validated multivariate chemometric models need the finalization to set the mechanistic QbD framework of process monitoring in relation to the product specification (real-time release and stability). Solid-state chemical and physical stability are integral parts of the pre-approval accelerated and long-term stability reports for new drug application filing. Sensitivity of solid-state techniques should be adequate to precisely identify any alteration of physical structure (mobility, miscibility, crystallinity, etc.) in finished product in comparison to the previously characterized intermediate ASD. Based on the nature of the product and behavior in the stability environment, mDSC and/or pXRD and vibrational-spectroscopy-based methods can be established as stability monitoring methods. This becomes often challenging as API in ASD-based final product is further diluted. The analytical capabilities of these standard techniques can be inadequate in case of consolidated finished dosage tablets containing ASD equivalent to API content $< 1\,\%$. The limit of detection and quantitation of chemometric NIR method for crystallinity spiked in indomethacin–PVP/VA ASD was recently found the lowest compared to pXRD and Raman methods in tablets with total drug content below 0.5 % (Palermo et al. 2012a, b). This forecasts a great utility of NIR method for online stability monitoring in ASD-based tablets of potent medications. The microstructures of amorphous films in coated tablets can significantly alter during storage that can impact the drug release profile which can be monitored using PALS. In general, regulators seek more characterization data on finished products than on the intermediate ASD and they also make more sense in correlating quality attributes of the finished products with its stability and in vivo data. Unfortunately, there seems to be very few scientific contributions on characterization of ASD-based finished dosage form with a great detail in comparison to the intermediate ASD.

The post-approval life cycle management of ASD-based products can become more challenging compared to ordinary crystalline formulation. Any alteration in physical structure of the product related to technology transfer and scale-up should fall under the scientifically characterized design space and should clearly reflect in the analytical data generated. The FDA recalls of nearly 100 solid oral dosages of small molecular API in past 2 years due to the physical defect or instability implied to criticality of product stability control (Recalls 2011–2013). The major specifications of current regulations are towards the chemical stability and degradations in the drug substances and product while limited guidance exists on the physical attributes. Moreover, predictability of physical stability of ASD-based products in ambient condition (shelf life) by routine accelerated stability testing is quantitatively poor and challenging. Therefore, different line extension products of ASD systems may need analytical data, specific to the particular products, to file the abbreviated applications.

A schematic overview of various structural characterization tools implementable at different stages of ASD-based product development is provided in Fig. 14.6.

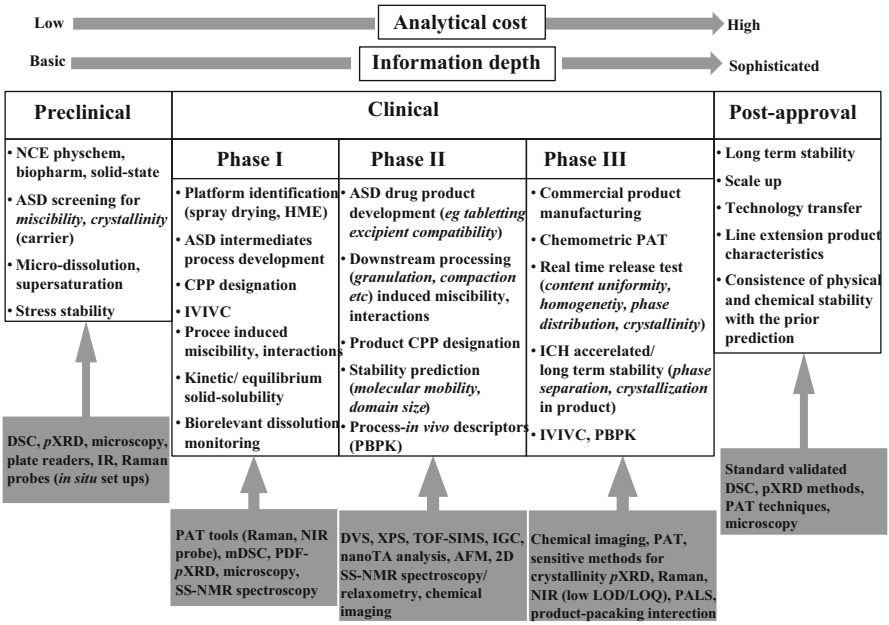

Fig. 14.6 Schematic presentation of utilization of various structural characterization tools implementable at different stages of ASD-based product development

The remaining techniques are summarized in Tables 14.1–14.9 at the end of the chapter.

Table 14.1 Description of various analytical tools utilized for the analysis of ASD

Techniques	Measuring principle/subtype
Dielectric relaxation spectroscopy (DRS) (Asami 2002; Kaatze 2013; Vassilikou-Dova and Kalogeras 2008)	The responses from orientational polarization within the analyte subjected to a varying external electric field Isochronal DRS: Constant frequency with temperature scanning, or varying time Isothermal frequency sweep broad-band DRS Varying frequency at constant temperature, measurement at different temperatures generates 3D profile
Thermally stimulated current (TSC) spectroscopy (Boutonnet-Fagegaltier et al. 2002; Gun'ko et al. 2007; Vassilikou-Dova and Kalogeras 2008)	Current released from analyte measured on linear reheating after polarization during quenching of the heated sample from the designated temperature under a constant DC electric field to a sub-ambient temperature ($\ll T_g$) Thermally stimulated depolarization current (TSDC) Thermal-windowing TSDC (TW-TSDC) Short temperature windows of polarization steps Thermally stimulated polarization current (TSPC) Current measured during first heating
Dynamic mechanical analysis (DMA) (Jones et al. 2012; Kalichevsky et al. 1992; Vassilikou-Dova and Kalogeras 2008)	Rheological behavior or mechanical stiffness (modulus) of the material subjected to an oscillating mechanical stress at selected frequencies Isochronal temperature sweep DMA (DMTA) More than 80 % application, constant frequency with temperature scanning, or varying RH Isothermal frequency sweep DMA Analogous to frequency sweep DRS
Solid-state vibrational spectroscopy/microscopy (Amigo 2010; Breitkreitz and Poppi 2012; Chen et al. 2011; Gendrin et al. 2008; Jørgensen et al. 2009; Kazarian and Ewing 2013; McIntosh et al. 2012; Pavia et al. 2001; Prats-Montalbán et al. 2012; Reich 2005; Van Eerdenbrugh and Taylor 2011; Zeitler et al. 2007)	Change in frequency of incident electromagnetic radiation due to the absorption or inelastic scattering of a portion resonant to the frequency of molecular, lattice or phonon vibration (stretching, bending, bending, rocking, wagging, scissoring, etc.) Middle infrared (MIR or IR) spectroscopy Asymmetric vibration of the polar bonds mediated by the alteration of the dipole moment Near infrared (NIR) spectroscopy Overtones and combinations of the fundamental vibrations Far infrared (terahertz, THz) spectroscopy Supramolecular vibrational, e.g., H-bonding, halogen-bonding or lattice/phonon vibrations Raman spectroscopy Scattering by non-isotropic change in molecular polarizability and leading to changes the rotational and vibrational motions Hyperspectral imaging/mapping Sequential collection of spectral data by locally scanning the selected areas within a static sample or simultaneous acquisitions of thousands of spectra resolved spatially PAT application Portable and temperature/pressure resistant fiber optics of NIR and Raman probes

Table 14.1 (continued)

Techniques	Measuring principle/subtype
Solid-state nuclear magnetic resonance (SS-NMR) techniques (Belton and Hills 1987; Courtier-Murias et al. 2012; Duer 2004; Fu and Sun 2011; Mantle 2011)	Interaction between a static magnetizing field and the spin angular momentum of spin active nuclei processing with angular frequency of a sample placed inside a radiofrequency (*rf*) coil ^{1}H SS-NMR spectroscopy Diverse local chemical environments makes a same proton nucleus experiences varying shielding effect against external field ^{13}C CP-MAS SS-NMR spectroscopy Magnetization transfer from abundant ^{1}H nuclei to rare ^{13}C(CP) and magic angle spinning (MAS) to nullify chemical shift anisotropy Heteronuclear (X = ^{15}N,^{19}F,^{17}O,^{31}P) SS-NMR spectroscopy Same as ^{13}C CP-MAS, but more selective 2D SS-NMR correlation spectroscopy Homo-nuclear (e.g.^{1}H-^{1}H) correlation (COSY), hetero-nuclear (^{1}H-X, X = ^{15}N,^{19}F,^{17}O,^{31}P) correlation (HETCOR) through- space and/or -bond dipolar coupling and nuclear interactions recorded by designed rf pulse sequences SS-NMR relaxometry Measurement, in time domain, of the rate of nuclear magnetization decay towards equilibrium following the excitation by an rf-pulse Longitudinal (spin-spin)-T_1(static)/$T_{1,}$ (rotating frame) relaxation time Transverse (spin lattice) - T_2 (from NMR line width) relaxation time NMR imaging Magnetic resonance (MRI), constant time (CTI) Spatial molecular mobility recorded via T_2 relaxation times of proton nuclei
Microscopic techniques (Carlton 2011; Dieing et al. 2011; Eddleston et al. 2010; Vitez et al. 1998)	Interaction of molecular solids with optical/electronic source resulting information on morphology, solid state Polarized light microscopy Identification of solid form based on birefringence and morphology Scanning electron microscopy (SEM) Focused electron beam scanned over the specimen surface under a high vacuum Penetrate the sample interior and the emitted electrons produces the specimen topography Transmission electron microscopy (TEM) Spatial variation of the inelastic interaction of electron beam while transmitting through a sample produces highly resolved image
Thermo-gravimetry (TGA; Giron et al. 2004)	Weight change of the sample as a function of temperature and/or time measured using a sensitive microbalance

Table 14.1 (continued)

Techniques	Measuring principle/subtype
Surface analytical techniques (Barnes et al. 2011; Brown and Vickerman 1984; Chehimi et al. 2011; Clark 1977; Harding et al. 2007; Ho and Heng 2013; Pollock and Hammiche 2001; Sitterberg et al. 2010; Thielmann and Levoguer 2002; Voelkel et al. 2009)	Atomic force microscopy (AFM) A sharp probe on a flexible cantilever tip (10–20 nm) scanned (contact mode, intermittent contact or tapping mode or non-contact mode) on a sample surface experiences attractive and repulsive forces thus yield high-resolution image and nano-mechanical information Localized thermal analysis (LTA; micro- or nano-thermal analysis) An AFM probe equipped with a thermal probe heats up sample resulting topographical imaging and thermal analysis of specific areas of the sample surface, sudden change in deflection of the heated cantilever indicates a thermal transition Time-of-flight secondary ion mass spectrometry (ToF-SIMS) Mass spectrometry of sample surface maps spatial compositional information: the distribution of compounds within 1–2 nm depth X-ray photoelectron spectroscopy (XPS) Low-energy X-ray irradiated on a sample surface under high vacuum allows quantitation of atomic concentration over a depth up to 10 nm Inverse gas chromatography (IGC) The retention behavior (volume, time) of a probe gas flowing at constant rate through a column packed with the solid sample yield information on surface interaction/energetics
Emerging techniques (Dlubek et al., 2007; Kissick et al., 2011; Magazu et al., 2011; Pansare et al., 2012; Zelkóa et al., 2006)	Positron annihilation lifetime spectroscopy (PALS) Molecular free volume (distribution) of a sample probed by the ortho positronium (o-Ps) formed by the parallel spin interaction of injected positron atom with the electron of the sample Second order nonlinear optical imaging of chiral crystals (SONICC) Selective images are produced by the detection of half the incident wavelength due to the occurrence of second harmonic generation by well-ordered chiral crystals Fluorescence resonance energy transfer (FRET) The extent of nonradiative energy transfer via long-range dipole–dipole coupling from excited fluorescent donor molecule to acceptor molecule is inversely related to the pair distance (3–10 nm) Neutron scattering Incoherent neutron scattering by the sample atoms provides information the self-dynamics such as mean square displacements and the onset of anharmonic motions of these atoms
Simultaneous tools (Dazzi et al. 2012; Feth et al. 2011; Ghita et al. 2008; Huang and Dali 2013; Pandita et al. 2012; Pili et al. 2010; Rahman et al. 2013)	Simultaneous multi-methodological measurement on a same sample, increases confidence on the data interpretation of complex systems DSC-TGA, DSC-XRD, DSC-Raman, DSC-FTIR, and DSC-NIR GVS-NIR AFM-IR

PAT process analytical technology

Table 14.2 Structural properties of ASD measurable by dielectric relaxation spectroscopy (DRS) and possible hurdles

Molecular mobility (Adrjanowicz et al. 2009, 2012; Bhugra et al. 2008; Bra's et al. 2008; Carpentier et al. 2006; Diogo and Moura-Ramos 2009; Havriliak and Negami 1967; Kaminski et al. 2011; Schönhals; Williams 2009)	Miscibility (Bhattacharya and Suryanarayanan 2011; Caron et al. 2010; Grzybowska et al. 2012; Kaminska et al. 2013; Korhonen et al. 2008; Roig et al. 2011; Tarek El and Roland 2007; Vassilikou-Dova and Kalogeras 2008; Zhang et al. 2004)	Crystallinty/crystallization (Alie et al. 2004; Bhattacharya and Suryanarayanan 2011; Bra's et al. 2008; Dantuluri et al. 2011; Gnutzmann et al. 2013; Grzybowska et al. 2012; Kaminski et al. 2011; Maheswaram et al. 2013; Wojnarowska et al. 2010)	Interference/limitations (Bhardwaj and Suryanarayanan 2011; Caron et al. 2010; Micko 2012; Vassilikou-Dova and Kalogeras 2008)
α-Process at T_g and other processes above T_g, and other sub-T_g relaxation processes (*JG*-, β-, γ-. . .)	Temperature scanning isochronal DRS exhibits composition-dependent T_g of blend as in DSC	Amorphous materials possess up to 10^8 times higher conductivity than crystalline	DC conductivity interferes the low frequency signals
Relaxation profiles obtained as loss peak in imaginary dielectric curve and as step jump of real permittivity line	Partial miscibility might exhibit multiple relaxation peaks overlaying or towards individual components, or display diverse relaxation rate even $> T_g$	Non-isothermal crystallization by isochronal temperature sweep DSC (cold crystallization and melting discernible as sudden drop and steep rise of static dielectric permittivity, respectively)	Crystallization onset predicted using DRS relaxation time in coupling model faster than the experimental time
Relaxation times are generally shorter than measured by thermal analysis	Molecularly mixed system show broader loss peak compared to individual peak	Isothermal crystallization above and below T_g can be studied by broadband DRS	Effect of water difficult to discern
Various model available to fit the non-Debye relaxation profiles	Width of loss peak also provide the measure of dynamic heterogeneity	Dielectric intensity/strength or α-peak decreases as crystallization progresses with time)	Exact identity of molecular relaxor needs complementary analysis
	Loss peak of some secondary processes can obscure with the stronger inter-component H-bonding in blend		Physical meaning of relaxation times parameters obtained by fitting DRS data by existing molecular mobility models still unclear
	DRS probes plasticization of selective motional process		

DSC differential scanning calorimetry

Table 14.3 Structural properties of ASD measurable by thermally stimulated current (TSC) spectroscopy and possible hurdles

Molecular mobility (Alie et al. 2004; Bhugra et al. 2008; Hirakura et al. 2007; Moura Ramos et al. 2002; Vassilikou-Dova and Kalogeras 2008; Viciosa et al. 2009)	Miscibility (Dong et al. 2008; Ghosh et al. 2011; Roig et al. 2011; Shmeis et al. 2004a, b)	Interference/limitations (Antonijevi'c et al. 2008; Dong et al. 2008; Jain et al. 2012; Shi et al. 2011)
Best resolution of the subtle sub-T_g local relaxation originating from rotational mobility of molecular dipoles	Increase in plasticization of loss peak with increasing a lower T_g drug content increases in ASD, T_g often resembles calorimetric T_g	Interference from space-charge peak (interfacial polarization signal), preconditioning can eliminate such effect
Peak of α-process at T_g, post-T_g signal from rigid amorphous fraction	Higher scatter of TW-TSDC peaks under a global peak indicates higher compositional heterogeneity	Non-Debye decay functions (e.g., KWW) is inappropriate to describe the TSDC relaxation process measured in temperature scanning mode
TW-TSDC deconvolutes a global peak of a particular motional process into ensemble of Debye peaks	TSPC would be able to measure initial structure of ASD with no need of thermal cleaning	Cleaning of thermal history disadvantageous to measure initial structure of sample by TSDC
Cooperative process identified by the convergence of individual relaxation times to a single point (compensation temperature)	Discrimination of free versus plasticizing water in ASD	

ASD amorphous solid dispersions, *TW-TSDC* thermal-windowing thermally stimulated discharge current

Table 14.4 Structural properties of ASD measurable by dynamic mechanical analysis (DMA) and possible hurdles

Molecular mobility (Andronis and Zografi 1997; Jones et al. 2012; Kalichevsky et al. 1992; Vyazovkin and Dranca 2006)	Miscibility (Abiad et al. 2010; Fadda et al. 2010; Hoppu et al. 2009; Jones et al. 2012; Labuschagne et al. 2010; Lamm et al. 2012; Liu et al. 2012; Poirier-Brulez et al. 2006; Suknunthaa et al. 2012; Yang et al. 2011)	Crystallinty/crystallization (Gupta and Bansal 2005; Soutari et al. 2012)	Interference/limitations (Abiad et al. 2010; Ayenew et al. 2012; Suknunthaa et al. 2012)
Detects from a relaxation to subtle sub-T_g processes that show otherwise negligible change in heat capacity (β,γ etc.)	Complementary to DSC, symmetrical and narrower loss peak for miscible system, multiple loss peaks for highly heterogeneous system	Employs the quantifiable difference in mechanical response of crystalline and amorphous state of a material	Need of a special sample geometry and amount, difficult to mount powder
$\hat{I}$'-peak not interfered (e.g., by DC in DRS)	Solid solubility estimation from melt rheology	Monitoring amorphous-to-crystalline transition as a function of temperature and/or time	Brittle ASD with higher drug content inappropriate for DMA analysis
Activation energy for α,β process between that measured by DRS and TSC	T_g measured higher than calorimetric T_g		ASD compact preparation may risk the alteration of the physical structure
	Composition-dependent hardness, reduced, and storage moduli obtained by nano-DMA provide miscibility data		

Table 14.5 Vibrational spectroscopic and microscopic analysis of ASD structure and possible hurdles

Miscibility and molecular interactions (Andrews et al. 2010; Breitkreitz and Poppi 2012; Hartshorn et al. 2013; Hédoux et al. 2011; Marsac et al. 2010; Padilla et al. 2010; Paudel et al. 2012; Qian et al. 2010; Rumondor et al. 2011; Wegiel et al. 2012; Zeitler et al. 2007)	Crystallinty/crystallization (Chan et al. 2004; Hédoux et al. 2011; Hédoux et al. 2009; Kao et al. 2012; Palermo et al. 2012a, b; Priemel et al. 2012; Sinclair et al. 2011; Vehring et al. 2012)	Interference/limitations (Gendrin et al. 2008; Jørgensen et al. 2009; Matero et al. 2013; Taylor et al. 2001)
IR, Raman scrutinize homo/heteromolecular interaction (H-bonding, dipolar interaction), higher sensitivity of NIR for H-bonding (OH overtones/combinations)	Amorphization generally weakens many intermolecular interactions while strengthens some	Overlapping peaks need deconvolution and multivariate data analysis for quantification, multicomponent image analysis requires chemometric methods
Various structural information from band shift, relative peak intensities and/or width, e.g., drug–polymer H-bonding (red shift), monomer–multimer ratio of API	Relative crystallinity can be quantified from the ratio of peak intensities of vibrational bands unique to amorphous and crystalline forms or the ratio of peak width of partially to completely crystalline samples of IR or Raman spectra	Contribution from the alteration of the specific molar absorbance on newer bands (e.g., drug–polymer interactions) difficult to account for absolute quantification
Homo- (drug–drug, polymer–polymer) versus heteromolecular (drug–polymer) interactions, conformational states, dipolar self- and interassociation, phase-separation	Low-frequency (LF) Raman region sensitive to amorphous form preparation method (polyamorphism), associated to the excess quasi-harmonic vibrational density of states of amorphous materials representing the feeble phonon signature of underlying the crystal	Particle size, distribution and shape of sample require crucial control for reproducibility
Variable temperature/RH Raman or FTIR for heat/moisture-induced molecular demixing	Spectral monitoring of crystallization during storage, etc., LF Raman susceptibility presents superior sensitivity to the phonon peaks from lattice vibration thus detect nanocrystallites (30 Å) even in low API content (2–5 %)	MIR region highly susceptible to the interference from moisture peaks thus poses hurdle for hygroscopic samples
Time-domain THz measurement for molecular mobility studies		Raman signals are less affected by water peaks but confronted by fluorescence related artifacts from elastic scattering

Table 14.5 (continued)

Miscibility and molecular interactions (Andrews et al. 2010; Breitkreitz and Poppi 2012; Hartshorn et al. 2013; Hédoux et al. 2011; Marsac et al. 2010; Padilla et al. 2010; Paudel et al. 2012; Qian et al. 2010; Rumondor et al. 2011; Wegiel et al. 2012; Zeitler et al. 2007)	Crystallinty/crystallization (Chan et al. 2004; Hédoux et al. 2011; Hédoux et al. 2009; Kao et al. 2012; Palermo et al. 2012a, b; Priemel et al. 2012; Sinclair et al. 2011; Vehring et al. 2012)	Interference/limitations (Gendrin et al. 2008; Jørgensen et al. 2009; Matero et al. 2013; Taylor et al. 2001)
Vibrational (MIR, NIR, Raman, THz) microscopy (imaging/mapping) serves for fast and unambiguous quantification of the different solid forms of API in matrix, high signal-to-noise ratio and spatiochemical resolution Physical states and distribution API in matrix, studies of spatiotemporal (in situ) phase transitions and real-time structural evolution (e.g., during dissolution) Selective identification of the solid-state of API in formulations in THz spectra due to THz transparency of most pharmaceutical excipients Stronger scattering aromatic APIs than aliphatic polymers provides better structural contrast in Raman imaging and also lesser interference by water	Loss of phonon vibration results in the diffuse THz spectrum for the amorphous state enables identification and quantitation of crystal	NIR bands are often too diffused for quantitative use for higher number of constituents in ASD
NIR/Raman as PAT tools (Almeida et al. 2012; Alonzo et al. 2010; de Veij et al. 2009; Saerens et al. 2011, 2012; Smith-Goettler et al. 2011; Tumuluri et al. 2008; Wahl et al. 2013)		
Expeditious and non-destructive PAT tools for remote sampling *On-line* monitoring of solid-state phase transformations in dry *or su*spended samples during manufacturing (e.g., by hot melt extrusion) Monitoring solid- and solution-mediated transformations (e.g., nucleation, crystallization) during dissolution of ASD		

API active pharmaceutical ingredient, *FTIR* Fourier transform infrared spectroscopy, *NIR* near-infrared spectroscopy, *PAT* process analytical technology, *THz* terahertz

Table 14.6 Structural characterization of ASD by solid-state nuclear magnetic resonance (SS-NMR) spectroscopy and relaxometry and possible hurdles

Molecular mobility (Apperley et al. 2005; Aso et al. 2000; Benmore et al. 2013; Carpentier et al. 2006; Geppi et al. 2008; Ito et al. 2010)	Miscibility and drug–polymer interaction (Aso and Yoshioka 2006; Aso et al. 2002, 2007, 2009; Brettmann et al. 2012a, b; Chen et al. 2005; Forster et al. 2003; Geppi et al. 2008; Klama 2010; Pham et al. 2010; Tatton et al. 2013; Vogt et al. 2011, 2013)	Crystallinty/crystallization (Aso et al. 2009; Dahlberg et al. 2011; Geppi et al. 2008; Offerdahl et al. 2005; Seliger and Žagar 2013; Urbanova et al. 2013; Vogt and Williams 2012; Vogt et al. 2011)	Interference/limitations (Geppi et al. 2008; Pham et al. 2010; Schantz et al. 2009; Vogt et al. 2011)
Record motional process in a molecule within wider time scale (10^{-11}–10^{-4} s)	H-bonding results deshielding, intra and intermolecular interaction of API in matrix, H-bonding configurations (*groups, H-bond distance*)	Crystallinity determination based on different dynamics/spectral features of amorphous (faster, disordered) and crystalline (slower, ordered) fraction, T_1 relaxation highly sensitive to the crystalline state	Risk of crystallization of during longer measurement time necessary for T_1
Identification of dynamics of a particular molecular fractions with diverse mobility	Wider frequency range ^{13}C CP SS-NMR eases interpretation	Analysis of NMR line width versus delay time (T_2 profiles) using Gaussian–Lorentzian function (*Gaussian part: crystalline and Lorentzian: amorphous fraction*) for partially crystallinity	Ambiguity about the source of biphasic spin relaxation decay profile (due to *dynamic heterogeneity and/or heteronuclear coupling*)
T_1-from local/rapid, T_1-from α-like process and T_2- sensitive to local motions	Information on the H-bonding geometry nuclear quadrupolar moment and EFG at quadrupolar nuclei (spin > 1/2) such as^{14}N,^{35}Cl,^{17}O	Variable temperature NMR relaxometry to study non-isothermal crystallization	Detection of heterogeneity based on relaxometry limited to the API and polymers having different independent relaxation times as (*analogous to identical T_g problem for DSC*)

Table 14.6 (continued)

Molecular mobility (Apperley et al. 2005; Aso et al. 2000; Benmore et al. 2013; Carpentier et al. 2006; Geppi et al. 2008; Ito et al. 2010)	Miscibility and drug–polymer interaction (Aso and Yoshioka 2006; Aso et al. 2002, 2007, 2009; Brettmann et al. 2012a, b; Chen et al. 2005; Forster et al. 2003; Geppi et al. 2008; Klama 2010; Pham et al. 2010; Tatton et al. 2013; Vogt et al. 2011, 2013)	Crystallinty/crystallization (Aso et al. 2009; Dahlberg et al. 2011; Geppi et al. 2008; Offerdahl et al. 2005; Seliger and Žagar 2013; Urbanova et al. 2013; Vogt and Williams 2012; Vogt et al. 2011)	Interference/limitations (Geppi et al. 2008; Pham et al. 2010; Schantz et al. 2009; Vogt et al. 2011)
Richer information from variable temperature and hetero-nuclear relaxometry (e.g., ^{19}F T_1/T_1 nearest neighbor distance)	Molecular mechanism of miscibility from 2D-correlation contours (strength, i.e., distance of drug–polymer H-bonding)	Convoluted spectral profile of partially crystalline dispersions due to overlapping sharp signals of crystalline fraction and the broad peaks of the amorphous fraction	Expensive, time and resource intensive technique
T_1- and T_1-relaxation times of abundant nuclei-dynamic heterogeneity	Hetero-nuclear correlation (e.g., ^{1}H-^{19}F) more selective, ^{17}O SS-NMR susceptible to split of drug–drug H-bonding by drug–polymer mixing	Minimal MVA or gravimetric calibration for quantitatively specific high-resolution CP-NMR	Best results by NMR imaging only of static sample, dynamic dissolution conditions generate complexity
	Qualitative drug–polymer miscibility from the observed spectral alterations (*peak shift, shielding/deshielding, broadening*)	Up to 1 % API crystallinity detectable in polymeric mixtures	
	Estimates of the upper boundary of domain size of inhomogeneity in ASD from magnetization spin-diffusion length (from ^{1}H $T_1/T_{1\rho}$ times)	Crystallization monitoring > T_g alternatively by nuclear quadrupole double resonance	

Table 14.6 (continued)

Molecular mobility (Apperley et al. 2005; Aso et al. 2000; Benmore et al. 2013; Carpentier et al. 2006; Geppi et al. 2008; Ito et al. 2010)	Miscibility and drug–polymer interaction (Aso and Yoshioka 2006; Aso et al. 2002, 2007, 2009; Brettmann et al. 2012a, b; Chen et al. 2005; Forster et al. 2003; Geppi et al. 2008; Klama 2010; Pham et al. 2010; Tatton et al. 2013; Vogt et al. 2011, 2013)	Crystallinty/crystallization (Aso et al. 2009; Dahlberg et al. 2011; Geppi et al. 2008; Offerdahl et al. 2005; Seliger and Žagar 2013; Urbanova et al. 2013; Vogt and Williams 2012; Vogt et al. 2011)	Interference/limitations (Geppi et al. 2008; Pham et al. 2010; Schantz et al. 2009; Vogt et al. 2011)
	For phase-separated ASD exhibiting two distinct sets of relaxation times, separated domain size estimated from respective $T_1/T_{1\rho}$ times		
	Domain size of API in intimately mixed ASD (≤ 10 nm) deduced using T_2 relaxation times (*amorphous cluster versus molecular dispersion*)		
	2D-NMR through-space hetero-nuclear dipolar coupling distance to directly probe molecular proximity		
NMR imaging *(Dahlberg et al. 2011; Gladden and Sederman 2013; Langham et al. 2012; Mantle 2013)*			
Cross-section image from inside of an opaque (undisturbed) specimen Series of in situ temporal imaging of kinetic events during dissolution process viz., drug release and/or (re)crystallization, polymer mobilization, medium ingress, etc. Local distribution of nuclear spin density Spatial mapping of the associated component (API, polymer or dissolution medium) using T_2-relaxation times or self-diffusion coeffic$_i$ent of a specific nucleus within a sample volume Mutual interactions with other components and translation motions			

ASD amorphous solid dispersions, *API* active pharmaceutical ingredient, *MVA* multivariate analysis, *EFG* electric field gradient, *DSC* differential scanning calorimetry

Table 14.7 Light and electron microscopic analysis of morphology and microstructure of ASD

Microscopy	Structural information	Interference/limitations
Polarized light microscopy (Cai et al. 2011; Kestur and Taylor 2010, 2013; Konno and Taylor 2006; Yang and Gogos 2013)	Rapid detection of crystals based upon birefringence as completely amorphous sample lacks the same Nucleation and crystal growth kinetics (number, size and fractal) at variable temperature and/or RH Surface and bulk crystallization represented by uncovered and covered sample, respectively Morphology and aspect ratio of crystals, particle/crystal size, and distribution Detection of melting, dehydration, crystallization, degradation, etc., by hot stage microscopy	Insufficient illumination of trace/small crystallites dispersed in polymer matrix Isotropic crystal (e.g., cubic) non-birefringent Some amorphous polymer also exhibit virtual birefringence due to shear induced deformation Semiquantitative
Scanning electron microscopy (SEM) (Karavas et al. 2007a, b; Qi et al. 2010a, b)	Morphological inspections of nanostructures and amorphous systems with high (nm) spatial resolution under several thousand times magnification Rapid detection of surface crystal (size, number, and shape), suitable for the analysis of particulate and bulk level characteristics (particle size, crystal morphology, agglomerates) Surface topography, rugosity, etc. Chemical distribution map of the location and heterogeneity of different components using energy-dispersive X-ray spectroscopy (EDS)	Possible electronic ablation of labile sample surface Inadequate for the detailed analysis of amorphous phase structure (e.g. *phase separation, domain/cluster size/shape*) Inherent need of smooth/flat (microtomic) sample surface for quantitative applications by EDS Dissimilar drug–polymer elemental composition required for discriminatory EDS mapping
Transmission electron microscopy (TEM) (Bikiaris et al. 2005; De Zordi et al. 2012; Karavas et al. 2007a, b; Ma et al. 2013; Nakayama et al. 2009)	Ultimate spatial resolution for analyzing compositional heterogeneities, density variations, grain boundaries, etc. Reasonable contrast provided by hetero-elemental API for the measurement of the dimension of amorphous drug nano-clusters dispersed in the polymer matrix TEM/EDS for drug–polymer miscibility, i.e., molecularly mixed systems appear as a continuous matrix without elemental localization (lack of local elemental spikes) Spatial distinction of nanoscopic physical structure among amorphous, crystalline, and other mesophases in heterogeneous polymeric dispersion using selective negative staining of unsaturated API by heavy metal oxides (e.g., OsO_4) over excipients Characterization of polymorphs, nanocrystals, salts, co-crystals, etc.	Electron beam damage for some samples Impedingly tedious sample preparation Exotic elemental marker (considerable elemental dissimilarity between API and polymer) required for heterogeneity detection Ultimate safety required to handle the toxic staining agents

RH reversing heat

Table 14.8 Micro-/nano-structure analysis of ASD surface

Surface analytical tools	Structural information	Interference/limitations
Atomic force microscopy (AFM) (Lauer et al. 2011, 2013; Meeus et al. 2013; Qi et al. 2013a, b)	Surface nanoscopic phase imaging (*spatial phase/chemical nano-heterogeneities*) and nanometric topography imaging of ASD, dimension of surface phase separation Phase contrast in heterogeneous system due to more adhesive drug-rich than the polymer-rich domains Colloidal AFM for drug–carrier adhesion force measurement Local mechanical properties (viscoelasticity, Young's modulus, surface free energy, stiffness, etc.)	Damage of soft polymeric samples Smoother sample preferred as access to a very small area (*relatively smaller cantilever size than the particle curvature*) produce erroneous surface rugosity Interference of phase imaging results by the variations in sample-probe contact exerted by nano-topography
Localized thermal analysis (LTA) (Meeus et al. 2012; Meeus et al. 2013; Meng et al. 2012; Zhang et al. 2009)	Thermal transition mapping: softening temperature, T_g, melting at surface (âˆ¼10–100 nm), markedly different T_g, T_m from bulk (by DSC; e.g., *reduced melting of surface crystals*) Local mapping of miscibility (spatial T_g distribution) and the physical state of sample surface, capturing early onset of instability (nano phase separation), 3D topology/thermal conductivity mapping at the surface Analysis on inter-particulate composition in individual powder particle	Due to faster heating rates than DSC difficult to compare with latter Very thin shell-core structures difficult to analyze (more noises) Semi-quantitative analysis, tedious calibration
Time-of-flight secondary ion mass spectrometry (ToF-SIMS) (Meeus et al. 2013; Scoutaris et al. 2012; Shard et al. 2009)	Analysis of surface chemical composition of a sample (*top 1–2 nm layer*) Mapping of spatial surface distribution of mixture components, 3D chemical distribution and miscibility, relative drug distribution in multi-polymeric system Depth profiling by surface sputtering (*removing defined surface monolayers*)	Spatial resolution limits the estimation of phase-separated domain

Table 14.8 (continued)

Surface analytical tools	Structural information	Interference/limitations
X-ray photoelectron spectroscopy (XPS) (Baer et al. 2011; Dahlberg et al. 2008; Maniruzzaman et al. 2013; Meeus et al. 2013)	Quantitative surface chemical composition analysis based on atomic concentration Profiling surface segregation (enrichment or depletion) of API and polymer in ASD particles Angle-resolved analysis of top surface layer, quantitative depth profiling of formulations Indication of drug–polymer interactions by spectral shift or new peaks	Spatial resolution around 1 μm for imaging Limited to drug–polymer with dissimilar elemental composition
Inverse gas chromatography (IGC) (Hasegawa et al. 2009; Ke et al. 2012; Lim et al. 2013; Miyanishi et al. 2013; Otte et al. 2012)	Surface molecular mobility, surface energy (dispersive, acidic, basic), and heterogeneity (disorder) Surface acidity/basicity (H-bond donor or acceptor number) Surface cohesion energy density, Flory–Huggins interaction parameter Surface crystallinity, RH-dependent surface T_g	Adsorption of probe gas on solid sample can interfere equilibrium data, reproducibility can be affected by the subtle change in sample porosity, texture, etc. Possible phase separation/crystallization during analysis (due to high column pressure) not clear

ASD amorphous solid dispersions, *API* active pharmaceutical ingredient, *AFM* atomic force microscopy, *RH* reversing heat

Table 14.9 Some emerging and potential analytical applications for the advanced characterization of ASD

Emerging/potential tools	Structural information	Interference/limitations
Positron annihilation lifetime spectroscopy (PALS) (Antal et al. 2013; Bölcskei et al. 2011; Chieng et al. 2013a, b; Gottnek et al. 2013; Szabó et al. 2011; Szente et al. 2009; Zelkóa et al. 2006)	Very sensitive analysis of local and global molecular mobility based on free volume change Change in free volume owing to structural cross linking by H-bond formation in ASD Miscibility derived from change in number, size (distribution) of molecular holes as a function of API content in ASD Water–solid interaction	Relatively novel application in ASD area Requires further exploration
Second order nonlinear optical imaging of chiral crystals (SONICC) (Kestur et al. 2012; Kissick et al. 2011; Toth et al. 2012; Wanapun et al. 2011)	Qualification of crystallinity and size distribution of trace chiral crystal in an amorphous matrix Extremely sensitive (4 ppm) of crystallinity for some chiral crystal systems Imaging of nanocrystal (90 nm) in polymeric matrix Potential utility for monitoring early stage nucleation/crystal growth from amorphous system	Limited to the chiral crystals Requires further exploration
Fluorescence resonance energy transfer (FRET) (van Drooge et al. 2006)	Study of miscibility in product with low drug content (0.5–1 %w/w) Estimation of domain size and identification of molecular cluster to dispersion possible Selective	Not applicable for high drug-loading system as API molecular proximity below FRET distance Fluorescent properties required and FRET should occur
Neutron scattering (Bordallo et al. 2012; Lerbret et al. 2012; Magazù et al. 2008; Magazù et al. 2010; Qi et al. 2013a, b)	Molecular dynamics and structural relaxation of multicomponent amorphous systems Small-angle neutron scattering for polymer–surfactant interaction during dissolution of ternary ASD	Sample preparation tedious Requires isotope labeling or enrichment

ASD amorphous solid dispersions, *API* active pharmaceutical ingredient

References

Abiad MG, Campanella OH, Carvajal MT (2010) Assessment of thermal transitions by dynamic mechanical analysis (DMA) using a novel disposable powder holder. Pharmaceutics 2:78–90

Adrjanowicz K, Wojnarowska Z, Wlodarczyk P, Kaminski K, Paluch M, Mazgalski J (2009) Molecular mobility in liquid and glassy states of Telmisartan (TEL) studied by broadband dielectric spectroscopy. Eur J Pharm Sci 38:395–404

Adrjanowicz K, Zakowiecki D, Kaminski K, Hawelek L, Grzybowska K, Tarnacka M, Paluch M, Cal K (2012) Molecular dynamics in supercooled liquid and glassy states of antibiotics: azithromycin, clarithromycin and roxithromycin studied by dielectric spectroscopy. Advantages given by the amorphous state. Mol Pharm 9:1748–1763

Alem N, Beezer AE, Gaisford S (2010) Quantifying the rates of relaxation of binary mixtures of amorphous pharmaceuticals with isothermal calorimetry. Int J Pharm 399:12–18

Alie J, Menegotto J, Cardon P, Duplaa H, Caron A, Lacabanne C, Bauer M, (2004) Dielectric study of the molecular mobility and the isothermal crystallization kinetics of an amorphous pharmaceutical drug substance. J Pharm Sci 93:218–233

Almeida A, Saerens L, De Beer T, Remon JP, Vervaet C (2012) Upscaling and in-line process monitoring via spectroscopic techniques of ethylene vinyl acetate hot-melt extruded formulations. Int J Pharm 439:223–229

Alonzo D, Zhang GZ, Zhou D, Gao Y, Taylor L (2010) Understanding the behavior of amorphous pharmaceutical systems during dissolution. Pharm Res 27:608–618

Amigo JM (2010) Practical issues of hyperspectral imaging analysis of solid dosage forms. Anal Bioanal Chem 398:93–109

Andrews GP, Abu-Diak O, Kusmanto F, Hornsby P, Hui Z, Jones DS (2010) Physicochemical characterization and drug-release properties of celecoxib hot-melt extruded glass solutions. J Pharm Pharmacol 62:1580–1590

Andronis V, Zografi G (1997) Molecular mobility of supercooled amorphous indomethacin, determined by dynamic mechanical analysis. Pharm Res 14:410–414

Antal I, Kállai N, Luhn O, Bernard J, Nagy ZK, Szabó B, Zelkó IK (2013) Supramolecular elucidation of the quality attributes of microcrystalline cellulose and isomalt composite pellet cores. J Pharm Biomed Anal 84:124–128

Antonijevi'c MD, Craig DQM, Barker SA (2008) The role of space charge formation in the generation of thermally stimulated current (TSC) spectroscopy data for a model amorphous drug system. Int J Pharm 353:8–14

Apperley DC, Forster AH, Fournier R, Harris RK, Hodgkinson P, Lancaster RW, Rades T (2005) Characterisation of indomethacin and nifedipine using variable-temperature solid-state NMR. Magn Reson Chem 43:881–892

Asami K (2002) Characterization of heterogeneous systems by dielectric spectroscopy. Prog Pol Sci 27:1617–1659

Aso Y, Yoshioka S (2006) Molecular mobility of nifedipine–PVP and phenobarbital–PVP solid dispersions as measured by ^{13}C-NMR spin-lattice relaxation time. J Pharm Sci 95:318–325

Aso Y, Yoshioka S, Kojima S (2000) Relationship between the crystallization rates of amorphous nifedipine, phenobarbital, and flopropione, and their molecular mobility as measured by their enthalpy relaxation and ^{1}H NMR relaxation times. J Pharm Sci 89:408–416

Aso Y, Yoshioka S, Zhang J, Zografi G (2002) Effect of water on the molecular mobility of sucrose and poly(vinylpyrrolidone) in a colyophilized formulation as measured by ^{13}C-NMR relaxation time. Chem Pharm Bull 50:822–826

Aso Y, Yoshioka S, Miyazaki T, Kawanishi T, Tanaka K, Kitamura S, Takakura A, Hayashi T., Muranushi N. (2007) Miscibility of nifedipine and hydrophilic polymers as measured by ^{1}H-NMR spin-lattice relaxation. Chem Pharm Bull 55:1227–1231

Aso Y, Yoshioka S, Miyazaki T, Kawanishi T (2009) Feasibility of ^{19}F-NMR for assessing the molecular mobility of flufenamic acid in solid dispersions. Chem Pharm Bull 57:61–64

Atassi F, Mao C, Masadeh AS, Byrn SR (2010) Solid-state characterization of amorphous and mesomorphous calcium ketoprofen. J Pharm Sci 99:3684–3697

Ayenew Z, Paudel A, Van den Mooter G (2012) Can compression induce demixing in amorphous solid dispersions? A case study of naproxen-PVP K25. Eur J Pharm Biopharm 81:207–213

Baer DR, Gaspar DJ, Nachimuthu P, Techane SD, Castner DG (2011) Application of surface chemical analysis tools for characterization of nanoparticles. Anal Bioanal Chem 983–1002

Baird JA, Taylor LS (2012) Evaluation of amorphous solid dispersion properties using thermal analysis techniques. Adv Drug Deliv Rev 64:396–421

Ball V, Maechling C (2009) Isothermal microcalorimetry to investigate non specific interactions in biophysical chemistry. Int J Mol Sci 10:3283–3315

Bansal SS, Kaushal AM, Bansal AK (2010) Enthalpy relaxation studies of two structurally related amorphous drugs and their binary dispersions. Drug Dev Ind Pharm 36:1271–1280

Barnes TJ, Kempson IM, Prestidge CA (2011) Surface analysis for compositional, chemical and structural imaging in pharmaceutics with mass spectrometry: a ToF-SIMS perspective. Int J Pharm 417:61–69

Bates S (2011) Amorphous materials: a structural perspective. Amorphous Workshop PPXRD–11

Bates S, Zografi G, Engers D, Morris K, Crowley K, Newman A (2006) Analysis of amorphous and nanocrystalline solids from their X-ray diffraction patterns. Pharm Res 23:2333–2349

Belton PS, Hills BP (1987) The effects of diffusive exchange in heterogeneous systems on N.M.R. line shapes and relaxation processes. Mol Phys 61:999–1018

Benmore CJ, R Weber JK, Tailor AN, Cherry BR, Yarger JL, Mou Q, Weber W, Neuefeind J, Byrn SR (2013) Structural characterization and aging of glassy pharmaceuticals made using acoustic levitation. J Pharm Sci 102:1290–1300

Bhardwaj SP, Suryanarayanan R (2011) Subtraction of DC conductivity and annealing: approaches to identify Johari-Goldstein relaxation in amorphous trehalose. Mol Pharmaceutics 8:1416–1422

Bhardwaj S, Suryanarayanan R (2013) Molecular mobility as a predictor of the water sorption by annealed amorphous trehalose. Pharm Res 30:714–720

Bhattacharya S, Suryanarayanan R (2009) Local mobility in amorphous pharmaceuticals—characterization and implications on stability. J Pharm Sci 98:2935–2953

Bhattacharya S, Suryanarayanan R (2011) Molecular motions in sucrose-PVP and sucrose-sorbitol dispersions: I. implications of global and local mobility on stability. Pharm Res 28:2191–2203

Bhugra C, Shmeis R, Krill S, Pikal M (2006) Predictions of onset of crystallization from experimental relaxation times I-correlation of molecular mobility from temperatures above the glass transition to temperatures below the glass transition. Pharm Res 23:2277–2290

Bhugra C, Shmeis R, Krill SL, Pikal MJ (2008a) Different measures of molecular mobility: comparison between calorimetric and thermally stimulated current relaxation times below Tg and correlation with dielectric relaxation times above T_g. J Pharm Sci 97:4498–4515

Bhugra C, Shmeis R, Krill SL, Pikal MJ (2008b) Prediction of onset of crystallization from experimental relaxation times. II. comparison between predicted and experimental onset times. J Pharm Sci 97:455–472

Bikiaris D, Papageorgiou GZ, Stergiou A, Pavlidou E, Karavas E, Kanaze F, Georgarakis M (2005) Physicochemical studies on solid dispersions of poorly water-soluble drugs: evaluation of capabilities and limitations of thermal analysis techniques. Thermochim Acta 439:58–67

Billinge SJL (2008) Nanoscale structural order from the atomic pair distribution function (PDF): there's plenty of room in the middle. J Solid State Chem 181:1695–1700

Billinge SJL, Dykhne T., Juhas P., Bozin E, Taylor R, Florence AJ, Shankland K (2010) Characterisation of amorphous and nanocrystalline molecular materials by total scattering. CrystEngComm 12:1366–1368

Blandamer MJ, Cullis PM, Engberts JBFN (1998) Titration microcalorimetry. J Chem Soc Faraday Trans 94:2261–2267

Boetker JP, Koradia V, Rades T, Rantanen J, Savolainen M (2012) Atomic pairwise distribution function analysis of the amorphous phase prepared by different manufacturing routes. Pharmaceutics 4:93–103

Bölcskei É, Süvegh K, Marekc GRT Jr, Pintye-Hódi K (2011) Testing of the structure of macromolecular polymer films containing solid active pharmaceutical ingredient (API) particles. Radiat Phys Chem 80:799–802

Bordallo HN, Zakharov BA, Boldyreva EV, Johnson MR, Koza MM, Seydel T, Fischer J (2012) Application of incoherent inelastic neutron scattering in pharmaceutical analysis: relaxation dynamics in phenacetin. Mol Pharm 9:2434–2441

Bøtker JP, Karmwar P, Strachan CJ, Cornett C, Tian F, Zujovic Z, Rantanen J, Rades T (2011) Assessment of crystalline disorder in cryo-milled samples of indomethacin using atomic pair-wise distribution functions. Int J Pharm 417:112–119

Boutonnet-Fagegaltier N, Menegotto J, Lamure A, Duplaa H, Caron A, Lacabanne C, Bauer M (2002) Molecular mobility study of amorphous and crystalline phases of a pharmaceutical product by thermally stimulated current spectrometry. J Pharm Sci 91:1548–1560

Brás AR, Noronha JP, Antunes AMM, Cardoso MM, Schönhals A, Affouard Fdr, Dionísio M, Correia NlT (2008) Molecular motions in amorphous ibuprofen as studied by broadband dielectric spectroscopy. J Phys Chem B 112:11087–11099

Breitkreitz MC, Poppi RJ (2012) Trends in Raman chemical imaging. Biomed Spectros Imag 1:159–183

Brettmann B, Bell E, Myerson A, Trout B (2012a) Solid-state NMR characterization of high-loading solid solutions of API and excipients formed by electrospinning. J Pharm Sci 101:1538–1545

Brettmann BK, Myerson AS, Trout BL (2012b) Solid-state nuclear magnetic resonance study of the physical stability of electrospun drug and polymer solid solutions. J Pharm Sci 101:2185–2193

Brown A, Vickerman JC (1984) Static SIMS for applied surface analysis. Surf Interface Anal 6:1–14

Buckton G, Darcy P (1999) Assessment of disorder in crystalline powders-a review of analytical techniques and their application. Int J Pharm 179:141–158

Burnett D, Malde N, Williams D (2009) Characterizing amorphous materials with gravimetric vapour sorption techniques. Pharma Tech Eur 21

Cai T, Zhu L, Yu L (2011) Crystallization of organic glasses: effects of polymer additives on bulk and surface crystal growth in amorphous nifedipine. Pharm Res 28:2458–2466

Calahan JL, Zanon RL, Alvarez-Nunez F, Munson EJ (2013) Isothermal microcalorimetry to investigate the phase separation for amorphous solid dispersions of AMG 517 with HPMC-AS. Mol Pharm 10:1949–1957

Carlton R (2011) Thermal microscopy, pharmaceutical microscopy. Springer, New York, pp 65–84

Caron V, Bhugra C, Pikal MJ (2010) Prediction of onset of crystallization in amorphous pharmaceutical systems: phenobarbital, nifedipine/PVP, and phenobarbital/PVP. J Pharm Sci 99:3887–3900

Caron V, Tajber L, Corrigan OI, Healy AM (2011) A comparison of spray drying and milling in the production of amorphous dispersions of sulfathiazole/polyvinylpyrrolidone and sulfadimidine/polyvinylpyrrolidone. Mol Pharm 8:532–542

Carpentier L, Decressain R, Gusseme A, Neves C, Descamps M (2006) Molecular mobility in glass forming fananserine: a dielectric, NMR, and TMDSC investigation. Pharm Res 23:798–805

Casarino P, Lavaggi P, Pedemonte E (1996) Heat of mixing in polymer blends based on poly(vinyl acetate). J Therm Anal Calorim 47:165–170

Chadha R, Bhandari S, Arora P, Chhikara R (2013) Characterization, quantification and stability of differently prepared amorphous forms of some oral hypoglycaemic agents. Pharml Dev Technol 18:504–514

Chakravarty P, Bates S, Thomas L (2013) Identification of a potential conformationally disordered mesophase in a small molecule: experimental and computational approaches. Mol Pharm 10:2809–2822

Chan KLA, Fleming OS, Kazarian SG, Vassou D, Chryssikos GD, Gionis V (2004) Polymorphism and devitrification of nifedipine under controlled humidity: a combined FT-Raman, IR and Raman microscopic investigation. J Raman Spectrosc 35:353–359

Chattoraj S, Bhugra C, Telang C, Zhong L, Wang Z, Sun C (2012) Origin of two modes of non-isothermal crystallization of glasses produced by milling. Pharm Res 29:1020–1032

Chehimi MM, Djouani F, Benzarti K (2011) XPS studies of multiphase polymer systems. In: Boudenne A, Ibos L, Candau Y, Thomas S (eds) Handbook of multiphase polymer systems, 1st edn. Wiley, Chichester, pp 585–637

Chen J-Z, Ranade SV, Xie X-Q (2005) NMR characterization of paclitaxel/poly (styrene-isobutylene-styrene) formulations. Int J Pharm 305:129–144

Chen Z, Lovett D, Morris J (2011) Process analytical technologies and real time process control a review of some spectroscopic issues and challenges. J Process Control 21:1467–1482

Chieng N, Cicerone MT, Zhong Q, Liu M, Pikal MJ (2013a) Characterization of dynamics in complex lyophilized formulations: II. Analysis of density variations in terms of glass dynamics and comparisons with global mobility, fast dynamics, and Positron Annihilation Lifetime Spectroscopy (PALS). Eur J Pharm Biopharm 85:197–206

Chieng N, Mizuno M, Pikal M (2013b) Characterization of dynamics in complex lyophilized formulations: I. Comparison of relaxation times measured by isothermal calorimetry with data estimated from the width of the glass transition temperature region. Eur J Pharm Biopharm 85:189–196

Clark DT (1977) ESCA applied to polymers, molecular properties. Springer, pp 125–188

Couchman PR, Karasz FE (1978) A classical thermodynamic discussion of the effect of composition on glass-transition temperatures. Macromolecules 11:117–119

Courtier-Murias D, Farooq H, Masoom H, Botana A, Soong R, Longstaffe JG, Simpson MJ, Maas WE, Fey M, Andrew B, Struppe J, Hutchins H, Krishnamurthy S, Kumar R, Monette M, Stronks HJ, Hume A, Simpson AJ (2012) Comprehensive multiphase NMR spectroscopy: basic experimental approaches to differentiate phases in heterogeneous samples. J Magn Reson 217:61–76

Crowley KJ, Zografi G (2002) Water vapor absorption into amorphous hydrophobic drug/poly(vinylpyrrolidone) dispersions. J Pharm Sci 91:2150–2165

Dahlberg C, Millqvist-Fureby A, Schuleit M (2008) Surface composition and contact angle relationships for differently prepared solid dispersions. Euro J Pharm Biopharm 70:478–485

Dahlberg C, Dvinskikh SV, Schuleit M, Furó I (2011) Polymer swelling, drug mobilization and drug recrystallization in hydrating solid dispersion tablets studied by multinuclear NMR microimaging and spectroscopy. Mol Pharm 8:1247–1256

Dantuluri AKR, Amin A, Puri V, Bansal AK (2011) Role of a-relaxation on crystallization of amorphous celecoxib above T_g probed by dielectric spectroscopy. Mol Pharm 8:814–822

Dazzi A, Prater CB, Hu Q, Chase DB, Rabolt JF, Marcott C (2012) AFM-IR: combining atomic force microscopy and infrared spectroscopy for nanoscale chemical characterization. Appl Spectrosc 66:1365–1491

de Veij M, Vandenabeele P, De Beer T, Remon JP, Moens L (2009) Reference database of Raman spectra of pharmaceutical excipients. J Raman Spectrosc 40:297–307

De Zordi N, Moneghini M, Kikic I, Grassi M, Del Rio Castillo AE, Solinas D, Bolger MB (2012) Applications of supercritical fluids to enhance the dissolution behaviors of Furosemide by generation of microparticles and solid dispersions. Eur J Pharm Biopharm 81:131–141

Descamps N, Palzer S, Zuercher U (2009) The amorphous state of spray-dried maltodextrin: sub-sub-T_g enthalpy relaxation and impact of temperature and water annealing. Carbohydr Res 344:85–90

Dieing T, Hollricher O, Toporski J, Haefele T, Paulus K (2011) Confocal Raman microscopy in pharmaceutical development, confocal raman microscopy. Springer, Berlin, pp 165–202

Diogo HP, Moura-Ramos JJ (2009) Secondary molecular mobility in amorphous ethyl cellulose: aging effects and degree of co-operativity. J Polymer Sci Part B: Polymer Phys 47:820–829

Dlubek G, Shaikh MQ, Krause-Rehberg R, Paluch M (2007) Effect of free volume and temperature on the structural relaxation in polymethylphenylsiloxane: a positron lifetime and pressure-volume-temperature study. J Chem Phys 126:24906

Dong Y-D, Boyd BJ (2011) Applications of X-ray scattering in pharmaceutical science. Int J Pharm 417:101–111

Dong Z, Chatterji A, Sandhu H, Choi DS, Chokshi H, Shah N (2008) Evaluation of solid state properties of solid dispersions prepared by hot-melt extrusion and solvent co-precipitation. Int J Pharm 355:141–149

Duer MJ (2004) Solid-state NMR spectroscopy. Wiley-Blackwell

Dykhne T, Taylor R, Florence A, Billinge SL (2011) Data requirements for the reliable use of atomic pair distribution functions in amorphous pharmaceutical fingerprinting. Pharm Res 28:1041–1048

Eddleston MD, Bithell EG, Jones W (2010) Transmission electron microscopy of pharmaceutical materials. J Pharm Sci 99:4072–4083

Ehtezazi T, Govender T, Stolnik S (2000) Hydrogen bonding and electrostatic interaction contributions to the interaction of a cationic drug with polyaspartic acid. Pharm Res 17:871–877

Fadda HM, Khanna M, Santos JC, Osman D, Gaisford S, Basit AW (2010) The use of dynamic mechanical analysis (DMA) to evaluate plasticization of acrylic polymer films under simulated gastrointestinal conditions. Eur J Pharm Biopharm 76 493–497

Farrow CL, Billinge SJL (2009) Relationship between the atomic pair distribution function and small-angle scattering: implications for modeling of nanoparticles. Acta Crystallograph Sec A 65:232–239

Feth MP, Jurascheck J, Spitzenberg M, Dillenz J, Bertele G, Stark H (2011) New technology for the investigation of water vapor sorption-induced crystallographic form transformations of chemical compounds: a water vapor sorption gravimetry-dispersive raman spectroscopy coupling. J Pharm Sci 100:1080–1092

Ford JL, Mann TE (2012) Fast-scan DSC and its role in pharmaceutical physical form characterisation and selection. Adv Drug Deliv Rev 64:422–430

Forster A, Apperley D, Hempenstall J, Lancaster R, Rades T (2003) Investigation of the physical stability of amorphous drug and drug/polymer melts using variable temperature solid state NMR. Die Pharmazie 58:761

Fu W, Sun P (2011) Solid state NMR study of hydrogen bonding, miscibility, and dynamics in multiphase polymer systems. Front Chem China 6173–189

Gaisford S (2005) Stability assessment of pharmaceuticals and biopharmaceuticals by isothermal calorimetry. Curr Pharm Biotechnol 6:181–191

Gaisford S (2012) Isothermal microcalorimetry for quantifying amorphous content in processed pharmaceuticals. Adv Drug Deliv Rev 64 431–439

Gaisford S, Verma A, Saunders M, Royall PG (2009) Monitoring crystallisation of drugs from fast-dissolving oral films with isothermal calorimetry. Int J Pharm 380:105–111

Gendrin C, Roggo Y, Collet C (2008) Pharmaceutical applications of vibrational chemical imaging and chemometrics: a review. J Pharm Biomed Anal 48:533–553

Geppi M, Mollica G, Borsacchi S, Veracini CA (2008) Solid-state NMR studies of pharmaceutical systems. Appl Spectrosc Rev 43:202–302

Ghita OR, Beard MA, McCabe J, Bottom R, Richmond J, Evans KE (2008) A study into first and second order thermal transitions of materials using spectral-DSC. J Mater Sci 43:4988–4995

Ghosh I, Snyder J, Vippagunta R, Alvine M, Vakil R, Tong W-Q, Vippagunta S (2011) Comparison of HPMC based polymers performance as carriers for manufacture of solid dispersions using the melt extruder. Int J Pharm 419:12–19

Giron D, Remy P, Thomas S, Vilette E (1997) Quantitation of amorphicity by microcalorimetry. J Therm Anal 48:465–472

Giron D, Mutz M, Garnier S (2004) Solid-state of pharmaceutical compounds. J Therm Anal Calorim 77:709–747

Gladden LF, Sederman AJ (2013) Recent advances in flow MRI. J Magn Reson 229:2–11

Gnutzmann T, Kahlau R, Scheifler S, Friedrichs F, Rossler EA, Rademann K, Emmerling F (2013) Crystal growth rates and molecular dynamics of nifedipine. CrystEngComm 15:4062–4069

Gordon M, Taylor JS (1952) Ideal copolymers and the second-order transitions of synthetic rubbers. I. non-crystalline copolymers. J Appl Chem 2:493–500

Gottnek M, Süvegh K, Pintye-Hódi K, Regdon G Jr (2013) Effects of excipients on the tensile strength, surface properties and free volume of Klucel® free films of pharmaceutical importance. Radiat Phys Chem 89:57–63

Graeser KA, Patterson JE, Zeitler JA, Gordon KC, Rades T (2009) Correlating thermodynamic and kinetic parameters with amorphous stability. Eur J Pharm Sci 37:492–498

Greco SP, Authelin J-R, Leveder C, Segalini A (2012) A practical method to predict physical stability of amorphous solid dispersions. Pharm Res 29:2792–2805

Greenspan L (1977) Humidity fixed points of binary saturated aqueous solutions. J Res Nat Bur Stand Sect A 81:89–96

Grisedale LC, Jamieson MJ, Belton PS, Barker SA, M Craig DQ (2010) Characterization and quantification of amorphous material in milled and spray-dried salbutamol sulfate: a comparison of thermal, spectroscopic, and water vapor sorption approaches. J Pharm Sci 100:3114–3129

Grzybowska K, Paluch M, Wlodarczyk P, Grzybowski A, Kaminski K, Hawelek L, Zakowiecki D, Kasprzycka A, Jankowska-Sumara I (2012) Enhancement of amorphous celecoxib stability by mixing it with octaacetylmaltose: the molecular dynamics study. Mol Pharm 9:894–904

Gun'ko VM, Zarko VI, Goncharuk EV, Andriyko LS, Turov VV, Nychiporuk YM, Leboda R, Skubiszewska-Zięba J, Gabchak AL, Osovskii VD, Ptushinskii YG, Yurchenko GR, Mishchuk OA, Gorbik PP, Pissis P, Blitz JP (2007) TSDC spectroscopy of relaxational and interfacial phenomena. Adv Colloid Interface Sci 131:1–89

Guns S, Kayaert P, Martens JA, Van Humbeeck J, Mathot V, Pijpers T, Zhuravlev E, Schick C, Van den Mooter G (2010) Characterization of the copolymer poly(ethyleneglycol-g-vinylalcohol) as a potential carrier in the formulation of solid dispersions. Eur J Pharm Biopharm 74:239–247

Guns S, Dereymaker A, Kayaert P, Mathot V, Martens J, Mooter G (2011) Comparison between hot-melt extrusion and spray-drying for manufacturing solid dispersions of the graft copolymer of ethylene glycol and vinylalcohol. Pharm Res 28:673–682

Gupta P, Bansal AK (2005) Devitrification of amorphous celecoxib. AAPS PharmSciTech 6:E223–E230

Hancock BC, Dalton CR (1999) The effect of temperature on water vapor sorption by some amorphous pharmaceutical sugars. Pharma Dev Technol 4:125–131

Hancock BC, Shamblin SL (2001) Molecular mobility of amorphous pharmaceuticals determined using differential scanning calorimetry. Thermochim Acta 380:95–107

Hancock B, Dalton C, Pikal M, Shamblin S (1998) A pragmatic test of a simple calorimetric method for determining the fragility of some amorphous pharmaceutical materials. Pharm Res 15 762–767

Hancock BC, Shalaev EY, Shamblin SL (2002) Polyamorphism: a pharmaceutical science perspective. J Pharm Pharm 54:1151–1152

Harding L, King WP, Dai X, Craig DQ, Reading M (2007) Nanoscale characterisation and imaging of partially amorphous materials using local thermomechanical analysis and heated tip AFM. Pharm Res 24:2048–2054

Hartshorn CM, Lee YJ, Camp CH, Liu Z, Heddleston J, Canfield N, Rhodes TA, Hight Walker AR, Marsac PJ, Cicerone MT (2013) Multicomponent chemical imaging of pharmaceutical solid dosage forms with broadband CARS microscopy. Anal Chem 85:8102–8111

Hasegawa S, Ke P, Buckton G (2009) Determination of the structural relaxation at the surface of amorphous solid dispersion using inverse gas chromatography. J Pharm Sci 98:2133–2139

Havriliak S, Negami S (1967) A complex plane representation of dielectric and mechanical relaxation processes in some polymers. Polymer 8:161–210

Hédoux A, Paccou L, Guinet Y, Willart J-Fo, Descamps M (2009) Using the low-frequency Raman spectroscopy to analyze the crystallization of amorphous indomethacin. Eur J Pharm Sci 38:156–164

Hédoux A, Guinet Y, Descamps M (2011) The contribution of Raman spectroscopy to the analysis of phase transformations in pharmaceutical compounds. Int J Pharm 417:17–31

Hirakura Y, Yamaguchi H, Mizuno M, Miyanishi H, Ueda S, Kitamura S (2007) Detection of lot-to-lot variations in the amorphous microstructure of lyophilized protein formulations. Int J Pharm 340:34–41

Ho R, Heng JYY (2013) A review of inverse gas chromatography and its development as a tool to characterize anisotropic surface properties of pharmaceutical solids. Kona Powder Part J 30:164–180

Hogan SE, Buckton G (2001) Water sorption/desorption-near IR and calorimetric study of crystalline and amorphous raffinose. Int J Pharm 227:57–69

Hoppu P, Hietala S, Schantz S, Juppo AM (2009) Rheology and molecular mobility of amorphous blends of citric acid and paracetamol. Euro J Pharm Biopharm 71:55–63

Huang J, Dali M (2013) Evaluation of integrated Raman-DSC technology in early pharmaceutical development: characterization of polymorphic systems. J Pharm Biomed Anal 86:92–99

ICHQ8(R2) (2009) ICH harmonised tripartite guideline (2009). Pharmaceutical Development

Ito A, Watanabe T, Yada S, Hamaura T, Nakagami H, Higashi K, Moribe K, Yamamoto K (2010) Prediction of recrystallization behavior of troglitazone/polyvinylpyrrolidone solid dispersion by solid-state NMR. Int J Pharm 383:18–23

Ivanisevic I (2010) Physical stability studies of miscible amorphous solid dispersions. J Pharm Sci 99:4005–4012

Ivanisevic I, Bates S, Chen P (2009) Novel methods for the assessment of miscibility of amorphous drug-polymer dispersions. J Pharm Sci 98:3373–3386

Ivanisevic I, McClurg RB, Schields PJ, Gad SC (2010) Uses of X-ray powder diffraction in the pharmaceutical industry: drug discovery, development, and manufacturing, pharmaceutical sciences encyclopedia. Wiley, pp 1–42

Jain D, Chandra LSS, Nath R, Ganesan V (2012) Low temperature thermal windowing (TW) thermally stimulated depolarization current (TSDC) setup. Meas Sci Technol 23:025603

Janssens S, Van den Mooter G (2009) Review: physical chemistry of solid dispersions. J Pharm Pharmacol 61:1571–1586

Janssens S, Zeure A, Paudel A, Humbeeck J, Rombaut P, Mooter G (2010) Influence of preparation methods on solid state supersaturation of amorphous solid dispersions: a case study with itraconazole and eudragit E100. Pharm Res 27:775–785

Jones DS, Tian Y, Abu-Diak O, Andrews GP (2012) Pharmaceutical applications of dynamic mechanical thermal analysis. Adv Drug Deliv Rev 64:440–448

Jørgensen AC, Strachan CJ, Pöllänen KH, Koradia V, Tian F, Rantanen J (2009) An insight into water of crystallization during processing using vibrational spectroscopy. J Pharm Sci 98:3903–3932

Kaatze U (2013) Measuring the dielectric properties of materials. Ninety-year development from low-frequency techniques to broadband spectroscopy and high-frequency imaging. Meas Sci Technol 24:12005

Kalichevsky MT, Jaroszkiewicz EM, Ablett S, Blanshard JMV, Lillford PJ (1992) The glass transition of amylopectin measured by DSC, DMTA and NMR. Carbohydr Polym 18:77–88

Kalogeras IM (2011) A novel approach for analyzing glass-transition temperature vs. composition patterns: application to pharmaceutical compound + polymer systems. Eur J Pharm Sci 42:470–483

Kaminska E, Adrjanowicz K, Kaminski K, Wlodarczyk P, Hawelek L, Kolodziejczyk K, Tarnacka M, Zakowiecki D, Kaczmarczyk-Sedlak I, Pilch J, Paluch M (2013) A new way of stabilization of furosemide upon cryogenic grinding by using acylated saccharides matrices. The role of hydrogen bonds in decomposition mechanism. Mol Pharm 10:1824–1835

Kaminski K, Adrjanowicz K, Wojnarowska Z, Grzybowska K, Hawelek L, Paluch M, Zakowiecki D, Mazgalski J (2011) Molecular dynamics of the cryomilled base and hydrochloride ziprasidones by means of dielectric spectroscopy. J Pharm Sci 100:2642–2657

Kao JY, McGoverin CM, Graeser KA, Rades T, Gordon KC (2012) Measurement of amorphous indomethacin stability with NIR and Raman spectroscopy. Vib Spectrosc 58:19–26

Karavas E, Georgarakis E, Sigalas MP, Avgoustakis K, Bikiaris D (2007a) Investigation of the release mechanism of a sparingly water-soluble drug from solid dispersions in hydrophilic

carriers based on physical state of drug, particle size distribution and drug-polymer interactions. Eur J Pharm Biopharm 66:334–347
Karavas E, Georgarakis M, Docoslis A, Bikiaris D (2007b) Combining SEM, TEM, and micro-Raman techniques to differentiate between the amorphous molecular level dispersions and nanodispersions of a poorly water-soluble drug within a polymer matrix. Int J Pharm 340:76–83
Karmwar P, Graeser K, Gordon KC, Strachan CJ, Rades T (2012) Effect of different preparation methods on the dissolution behaviour of amorphous indomethacin. Eur J Pharm Biopharm 80:459–464
Kawakami K (2011) Dynamics of ribavirin glass in the sub-T_g temperature region. J Phys Chem B 115:11375–11381
Kawakami K, Pikal MJ (2005) Calorimetric investigation of the structural relaxation of amorphous materials: evaluating validity of the methodologies. J Pharm Sci 94:948–965
Kawakami K, Usui T, Hattori M (2012) Understanding the glass-forming ability of active pharmaceutical ingredients for designing supersaturating dosage forms. J Pharm Sci 101:3239–3248
Kazarian SG, Ewing AV (2013) Applications of Fourier transform infrared spectroscopic imaging to tablet dissolution and drug release. Expert Opin Drug Deliv 10:1–15
Ke P, Hasegawa S, Al-Obaidi H, Buckton G (2012) Investigation of preparation methods on surface/bulk structural relaxation and glass fragility of amorphous solid dispersions. Int J Pharm 422:170–178
Kestur US, Taylor LS (2010) Role of polymer chemistry in influencing crystal growth rates from amorphous felodipine. CrystEngComm 12:2390–2397
Kestur US, Taylor LS (2013) Evaluation of the crystal growth rate of felodipine polymorphs in the presence and absence of additives as a function of temperature. Cryst Growth Des 13:4349–4354
Kestur US, Wanapun D, Toth SJ, Wegiel LA, Simpson GJ, Taylor LS (2012) Nonlinear optical imaging for sensitive detection of crystals in bulk amorphous powders. J Pharm Sci 101:4201–4213
Khougaz K, Clas S-D (2000) Crystallization inhibition in solid dispersions of MK-0591 and poly(vinylpyrrolidone) polymers. J Pharm Sci 89:1325–1334
Kissick DJ, Wanapun D, Simpson GJ (2011) Second-order nonlinear optical imaging of chiral crystals. Annu Rev Anal Chem (Palo Alto, Calif.) 4:419–437
Klama F (2010) NMR-studies of multi component solids. M. Sc. Dissertation, University of East Anglia, p 186
Koch MHJ, Bras W (2008) Synchrotron radiation studies of non-crystalline systems. Ann Rep Prog Chem Sect C 104:35–80
Konno H, Taylor LS (2006) Influence of different polymers on the crystallization tendency of molecularly dispersed amorphous felodipine. J Pharm Sci 95:2692–2705
Korhonen O, Bhugra C, Pikal MJ (2008) Correlation between molecular mobility and crystal growth of amorphous phenobarbital and phenobarbital with polyvinylpyrrolidone and L-proline. J Pharm Sci 97:3830–3841
Labuschagne PW, John MJ, Sadiku RE (2010) Investigation of the degree of homogeneity and hydrogen bonding in PEG/PVP blends prepared in supercritical CO_2: comparison with ethanol-cast blends and physical mixtures. J Supercrit Fluids 54:81–88
Laitinen R (2009) Title. University of Kuopio
Laitinen R, Suihko E, Toukola K, Björkqvist M, Riikonen J, Lehto VP, Järvinen K, Ketolainen J (2009) Intraorally fast-dissolving particles of a poorly soluble drug: preparation and in vitro characterization. Eur J Pharm Biopharm 71:271–281
Laitinen R, Suihko E, Bjorkqvist M, Riikonen J, Lehto V-P, Jarvinen K, Ketolainen J (2010) Perphenazine solid dispersions for orally fast-disintegrating tablets: physical stability and formulation. Drug Dev Ind Pharm 36:601–613
Lamm MS, Simpson A, McNevin M, Frankenfeld C, Nay R, Variankaval N (2012) Probing the effect of drug loading and humidity on the mechanical properties of solid dispersions with nanoindentation: antiplasticization of a polymer by a drug molecule. Mol Pharm 9:3396–3402

Langham ZA, Booth J, Hughes LP, Reynolds GK, Wren SAC (2012) Mechanistic insights into the dissolution of spray-dried amorphous solid dispersions. J Pharm Sci 101:2798–2810

Latsch S, Selzer T, Fink L, Kreuter Jr (2003) Crystallisation of estradiol containing TDDS determined by isothermal microcalorimetry, X-ray diffraction, and optical microscopy. Eur J Pharm Biopharm 56:43–52

Latsch S, Selzer T, Fink L, Horstmann M, Kreuter Jr (2004a) Use of isothermal heat conduction microcalorimetry, X-ray diffraction, and optical microscopy for characterisation of crystals grown in steroid combination-containing transdermal drug delivery systems. Eur J Pharm Biopharm 57:397–410

Latsch S, Selzer T, Fink L, Kreuter Jr (2004b) Determination of the physical state of norethindrone acetate containing transdermal drug delivery systems by isothermal microcalorimetry, X-ray diffraction, and optical microscopy. Eur J Pharm Biopharm 57:383–395

Lauer ME, Grassmann O, Siam M, Tardio J, Jacob L, Page S, Kindt JH, Engel A, Alsenz J (2011) Atomic force microscopy-based screening of drug-excipient miscibility and stability of solid dispersions. Pharm Res 28:572–584

Lauer ME, Siam M, Tardio J, Page S, Kindt JH, Grassmann O (2013) Rapid assessment of homogeneity and stability of amorphous solid dispersions by atomic force microscopy—from bench to batch. Pharm Res 30:1–13

Leane MM, Sinclair W, Qian F, Haddadin R, Brown A, Tobyn M, Dennis AB, (2013) Formulation and process design for a solid dosage form containing a spray-dried amorphous dispersion of ibipinabant. Pharm Dev Technol 18:359–366

Lechuga-Ballesteros D, Bakri A, Miller D (2003) Microcalorimetric measurement of the interactions between water vapor and amorphous pharmaceutical solids. Pharm Res 20:308–318

Lerbret A, Affouard Fdr, Hédoux A, Krenzlin S, Siepmann Jr, Bellissent-Funel M-C, Descamps M (2012) How strongly does trehalose interact with lysozyme in the solid state? Insights from molecular dynamics simulation and inelastic neutron scattering. J Phys Chem B 116:11103–11116

Liang LH, Zhao M, Jiang Q (2002) Melting enthalpy depression of nanocrystals based on surface effect. J Mater Sci Lett 21:1843–1845

Lim RTY, Ng WK, Widjaja E, Tan RBH (2013) Comparison of the physical stability and physicochemical properties of amorphous indomethacin prepared by co-milling and supercritical anti-solvent co-precipitation. J Supercr Fluids

Litvinov VM, Guns S, Adriaensens P, Scholtens BJR, Quaedflieg MP, Carleer R, Van den Mooter G (2012) Solid state solubility of miconazole in poly[(ethylene glycol)-g-vinyl alcohol] using hot-melt extrusion. Mol Pharm 9:2924–2932

Liu X, Yang P, Jiang Q (2007) Size effect on melting temperature of nanostructured drugs. Mater Chem Phys 103:1–4

Liu H, Zhang X, Suwardie H, Wang P, Gogos CG (2012a) Miscibility studies of indomethacin and Eudragit® E PO by thermal, rheological, and spectroscopic analysis. J Pharm Sci 101:2204–2212

Liu Y-M, Xu J-T, Fu Z-S, Fan Z-Q (2012b) Effect of phase separation on overall isothermal crystallization kinetics of PP/EPR in-reactor alloys. J Appl Polym Sci 127:1346–1358

Ma H, Choi D, Zhang Y-E, Tian H, Shah N, Chokshi H (2013) Evaluation on the drug-polymer mixing status in amorphous solid dispersions at the early stage formulation and process development. J Pharm Innov 8:163–174

Madsen IC, Scarlett NVY, Kern A (2011) Description and survey of methodologies for the determination of amorphous content via X-ray powder diffraction. Z Kristallogr 226:944–955

Magazù S, Maisano G, Migliardo F, Galli G, Benedetto A, Morineau D, Affouard Fdr, Descamps M (2008) Characterization of molecular motions in biomolecular systems by elastic incoherent neutron scattering. J Chem Phys 129:155103

Magazù S, Migliardo F, Affouard F, Descamps M, Telling MTF (2010) Study of the relaxational and vibrational dynamics of bioprotectant glass-forming mixtures by neutron scattering and molecular dynamics simulation. J Chem Phys 132:184512

Magazu S, Migliardo F, Benedetto A (2011) Elastic incoherent neutron scattering operating by varying instrumental energy resolution: principle, simulations, and experiments of the resolution elastic neutron scattering (RENS). Rev Sci Instrum 82:105111–105115

Maheswaram MP, Mantheni D, Perera I, Venumuddala H, Riga A, Alexander K (2013) Characterization of crystalline and amorphous content in pharmaceutical solids by dielectric thermal analysis. J Therm Anal Calorim 1–11

Maniruzzaman M, Morgan DJ, Mendham AP, Pang J, Snowden MJ, Douroumis D (2013) Drug-polymer intermolecular interactions in hot-melt extruded solid dispersions. Int J Pharm 443:199–208

Mantle MD (2011) Quantitative magnetic resonance micro-imaging methods for pharmaceutical research. Int J Pharm 417:173–195

Mantle MD (2013) NMR and MRI studies of drug delivery systems. Curr Opin Colloid Interface Sci 18:214–227

Marsac P, Shamblin S, Taylor L (2006) Theoretical and practical approaches for prediction of drug-polymer miscibility and solubility. Pharm Res 23:2417–2426

Marsac PJ, Rumondor ACF, Nivens DE, Kestur US, Stanciu L, Taylor LS (2010) Effect of temperature and moisture on the miscibility of amorphous dispersions of felodipine and poly(vinyl pyrrolidone). J Pharm Sci 99:169–185

Matero S, Den Berg Fv, Poutiainen S, Rantanen J, Pajander J (2013) Towards better process understanding: chemometrics and multivariate measurements in manufacturing of solid dosage forms. J Pharm Sci 102:1385–1403

McIntosh AI, Yang B, Goldup SM, Watkinson M, Donnan RS (2012) Terahertz spectroscopy: a powerful new tool for the chemical sciences? Chem Soc Rev 41:2072–2082

Meeus J, Chen X, Scurr DJ, Ciarnelli V, Amssoms K, Roberts CJ, Davies MC, Den Mooter Gv (2012) Nanoscale surface characterization and miscibility study of a spray-dried injectable polymeric matrix consisting of poly (lactic-co-glycolic-acid) and polyvinylpyrrolidone. J Pharm Sci 101:3473–3485

Meeus J, Scurr DJ, Amssoms K, Davies MC, Roberts CJ, Van den Mooter G (2013) Surface characteristics of spray-dried microspheres consisting of PLGA and PVP: relating the influence of heat and humidity to the thermal characteristics of these polymers. Mol Pharm 10:3213–3224

Meng J, Levina M, Rajabi-Siahboomi AR, Round AN, Reading M, Craig DQM 2012 The development of thermal nanoprobe methods as a means of characterizing and mapping plasticizer incorporation into ethylcellulose films. Pharm Res 29:2128–2138

Micko B (2012) title. University of Bayreuth

Miller D, Lechuga-Ballesteros D (2006) Rapid assessment of the structural relaxation behavior of amorphous pharmaceutical solids: effect of residual water on molecular mobility. Pharm Res 23:2291–2305

Miyanishi H, Nemoto T, Mizuno M, Mimura H, Kitamura S, Iwao Y, Noguchi S, Itai S (2013) Evaluation of crystallization behavior on the surface of nifedipine solid dispersion powder using inverse gas chromatography. Pharm Res 30:502–511

Moore MD, Wildfong PLD (2011) Informatics calibration of a molecular descriptors database to predict solid dispersion potential of small molecule organic solids. Int J Pharm 418:217–226

Moore M, Steinbach A, Buckner I, Wildfong PD (2009) A structural investigation into the compaction behavior of pharmaceutical composites using powder X-ray diffraction and total scattering analysis. Pharm Res 26:2429–2437

Moore M, Shi Z, Wildfong PD (2010) Structural interpretation in composite systems using powder X-ray diffraction: applications of error propagation to the pair distribution function. Pharm Res 27:2624–2632

Moura Ramos J, Correia Nl, Taveira-Marques R, Collins G (2002) The activation energy at T_g and the fragility index of indomethacin, predicted from the influence of the heating rate on the temperature position and on the intensity of thermally stimulated depolarization current peak. Pharm Res 19:1879–1884

Moynihan CT (1993) Correlation between the width of the glass transition region and the temperature dependence of the viscosity of high-T_g glasses. J Am Ceram Soc 76:1081–1087
Naelapää K, Boetker JP, Veski P, Rantanen J, Rades T, Kogermann K (2012) Polymorphic form of piroxicam influences the performance of amorphous material prepared by ball-milling. Int J Pharm 429:69–77
Nakayama S, Ihara K, Senna M (2009) Structure and properties of ibuprofen-hydroxypropyl methylcellulose nanocomposite gel. Powder Technol 190:221–224
Newman A, Engers D, Bates S, Ivanisevic I, Kelly RC, Zografi G (2008) Characterization of amorphous API:polymer mixtures using X-ray powder diffraction. J Pharm Sci 97:4840–4856
Ochsenbein P, Schenk KJ (2006) Crystallography for polymorphs, polymorphism. Wiley-VCH Verlag GmbH & Co. KGaA, pp 139–166
Offerdahl TJ, Salsbury JS, Dong Z, Grant DJW, Schroeder SA, Prakash I, Gorman EM, Barich DH, Munson EJ (2005) Quantitation of crystalline and amorphous forms of anhydrous neotame using ^{13}C CPMAS NMR spectroscopy. J Pharm Sci 94:2591–2605
O'Neill MAA, Gaisford S (2011) Application and use of isothermal calorimetry in pharmaceutical development. Int J Pharm 417:83–93
Otte A, Zhang Y, Carvajal MT, Pinal R (2012) Milling induces disorder in crystalline griseofulvin and order in its amorphous counterpart. CrystEngComm 14:2560–2570
Padilla AM, Ivanisevic I, Yang Y, Engers D, Bogner RH, Pikal MJ (2010) The study of phase separation in amorphous freeze-dried systems. Part I: Raman mapping and computational analysis of XRPD data in model polymer systems. J Pharm Sci 100:206–222
Palermo R, Short S, Anderson C, Tian H, Drennen J III (2012a) Determination of figures of merit for near-infrared, Raman and powder X-ray diffraction by net analyte signal analysis for a compacted amorphous dispersion with spiked crystallinity. J Pharm Innov 7:56–68
Palermo RN, Anderson CA, Drennen Iii JK (2012b) Review: use of thermal, diffraction, and vibrational analytical methods to determine mechanisms of solid dispersion stability. J Pharm Innov 7:2–12
Pandita SD, Wang L, Mahendran RS, Machavaram VR, Irfan MS, Harris D, Fernando GF (2012) Simultaneous DSC-FTIR spectroscopy: comparison of cross-linking kinetics of an epoxy/amine resin system. Thermochim Acta 543:9–17
Pansare VJ, Hejazi S, Faenza WJ, Prud'homme RK (2012) Review of long-wavelength optical and NIR imaging materials: contrast agents, fluorophores, and multifunctional nano carriers. Chem Mater 24:812–827
Patterson AL (1939) The Scherrer formula for X-ray particle size determination. Phys Rev 56:978–982
Paudel A, Mooter G (2012) Influence of solvent composition on the miscibility and physical stability of naproxen/PVP K 25 solid dispersions prepared by cosolvent spray-drying. Pharm Res 29:251–270
Paudel A, Van Humbeeck J, Van den Mooter G (2010) Theoretical and experimental investigation on the solid solubility and miscibility of naproxen in poly(vinylpyrrolidone). Mol Pharm 7:1133–1148
Paudel A, Nies E, Van den Mooter G (2012) Relating hydrogen-bonding interactions with the phase behavior of naproxen/PVP K 25 solid dispersions: evaluation of solution-cast and quench-cooled films. Mol Pharm 9:3301–3317
Paudel A, Worku ZA, Meeus J, Guns S, Van den Mooter G (2013a) Manufacturing of solid dispersions of poorly water soluble drugs by spray drying: formulation and process considerations. Int J Pharm 453:253–284
Paudel A, Loyson Y, Van den Mooter G (2013b) An investigation into the effect of spray drying temperature and atomizing conditions on miscibility, physical stability, and performance of naproxen–PVP K 25 solid dispersions. J Pharm Sci 102:1249–1267
Pavia DL, Lampman GM, Kriz GS (2001) Infrared spectroscopy in 'Introduction to spectroscopy': a guide for students of organic chemistry, 3rd edn. WB Saunders Co., Philadelphia

Penner EA (2013) Comparison of the new vapor sorption analyzer to the traditional saturated salt slurry method and the dynamic vapor sorption instrument. M. Sc. dissertation, University of Illinois

Perdana J, van der Sman RGM, Fox MB, Boom RM, Schutyser MAI (2014) Measuring and modelling of diffusivities in carbohydrate-rich matrices during thin film drying. J Food Eng 122:38–47

Pham TN, Watson SA, Edwards AJ, Chavda M, Clawson JS, Strohmeier M, Vogt FG (2010) Analysis of amorphous solid dispersions using 2D solid-state NMR and ^{1}H T_1 relaxation measurements. Mol Pharm 7:1667–1691

Pieters R, Miltner HE, Van Assche G, Van Mele B (2006) Kinetics of temperature-induced and reaction-induced phase separation studied by modulated temperature DSC. Macromol Symp 233:36–41

Pikal MJ, Chang L, Tang X (2004) Evaluation of glassy-state dynamics from the width of the glass transition: results from theoretical simulation of differential scanning calorimetry and comparisons with experiment. J Pharm Sci 93:981–994

Pili B, Bourgaux C, Amenitsch H, Keller G, Lepê tre-Mouelhi S, Desmaële D, Couvreur P, Ollivon M (2010) Interaction of a new anticancer prodrug, gemcitabine-squalene, with a model membrane: coupled DSC and XRD study. Biochim Biophys Acta (BBA) Biomembr 1798:1522–1532

Poirier-Brulez F, Roudaut G, Champion D, Tanguy M, Simatos D (2006) Influence of sucrose and water content on molecular mobilityin starch-based glasses as assessed through structureand secondary relaxation. Biopolymers 81:63–73

Pollock HM, Hammiche A (2001) Micro-thermal analysis: techniques and applications. J Phys D Appl Phys 34:R23

Prats-Montalbán JM, Jerez-Rozo JI, Romaach RJ, Ferrer A (2012) MIA and NIR chemical imaging for pharmaceutical product characterization. Chemometr Intell Lab Syst 117:240–249

Priemel PA, Grohganz H, Gordon KC, Rades T, Strachan CJ (2012) The impact of surface- and nano-crystallisation on the detected amorphous content and the dissolution behaviour of amorphous indomethacin. Euro J Pharm Biopharm 82:187–193

Puri V, Dantuluri AK, Bansal AK (2012) Barrier coated drug layered particles for enhanced performance of amorphous solid dispersion dosage form. J Pharm Sci 101:342–353

Qi S, Belton P, Nollenberger K, Clayden N, Reading M, Craig DM (2010a) Characterisation and prediction of phase separation in hot-melt extruded solid dispersions: a thermal, microscopic and NMR relaxometry study. Pharm Res 27:1869–1883

Qi S, Weuts I, De Cort S, Stokbroekx S, Leemans R, Reading M, Belton P, Craig DQ (2010b) An investigation into the crystallisation behaviour of an amorphous cryomilled pharmaceutical material above and below the glass transition temperature. J Pharm Sci 99:196–208

Qi S, Moffat JG, Yang Z (2013a) Early stage phase separation in pharmaceutical solid dispersion thin films under high humidity: improved spatial understanding using probe-based thermal and spectroscopic nanocharacterization methods. Mol Pharm 10:918–930

Qi S, Roser S, Edler K, Pigliacelli C, Rogerson M, Weuts I, Dycke F, Stokbroekx S (2013b) Insights into the role of polymer-surfactant complexes in drug solubilisation/stabilisation during drug release from solid dispersions. Pharm Res 30:290–302

Qian F, Huang J, Zhu Q, Haddadin R, Gawel J, Garmise R, Hussain M (2010) Is a distinctive single T_g a reliable indicator for the homogeneity of amorphous solid dispersion? Int J Pharm 395:232–235

Rahman Z, Siddiqui A, Khan MA (2013) Assessing the impact of nimodipine devitrification in the ternary cosolvent system through quality by design approach. Int J Pharm 455:113–123

Recalls U (2011–2013) http://www.fda.gov/Safety/Recalls/ArchiveRecalls/default.htm

Reich G (2005) Near-infrared spectroscopy and imaging: basic principles and pharmaceutical applications. Adv Drug Deliv Rev 57:1109–1143

Reutzel-Edens SM, Newman AW (2006) Physical characterization of hygroscopicity in pharmaceutical solids, polymorphism. Wiley-VCH Verlag GmbH & Co. KGaA, pp 235–258

Roe KD, Labuza TP (2005) Glass transition and crystallization of amorphous trehalose-sucrose mixtures. Int J Food Prop 8:559–574

Roig Fdr, Dantras E, Dandurand J, Lacabanne C (2011) Influence of hydrogen bonds on glass transition and dielectric relaxations of cellulose. J Phys D Appl Phys 44:045403

Roos YH (1995) Chapter 4—water and phase transitions, phase transitions in foods. Academic Press, San Diego, pp 73–107

Rumondor ACF, Taylor LS (2010) Application of partial least-squares (PLS) modeling in quantifying drug crystallinity in amorphous solid dispersions. Int J Pharm 398:155–160

Rumondor ACF, Marsac PJ, Stanford LA, Taylor LS (2009) Phase behavior of poly(vinylpyrrolidone) containing amorphous solid dispersions in the presence of moisture. Mol Pharm 6:1492–1505

Rumondor AF, Wikström H, Van Eerdenbrugh B, Taylor LS (2011) Understanding the tendency of amorphous solid dispersions to undergo amorphous-amorphous phase separation in the presence of absorbed moisture. AAPS PharmSciTech 12:1209–1219

Saerens L, Dierickx L, Lenain B, Vervaet C, Remon JP, Beer TD (2011) Raman spectroscopy for the in-line polymer-drug quantification and solid state characterization during a pharmaceutical hot-melt extrusion process. Eur J Pharm Biopharm 77:158–163

Saerens L, Dierickx L, Quinten T, Adriaensens P, Carleer R, Vervaet C, Remon JP, De Beer T (2012) In-line NIR spectroscopy for the understanding of polymer-drug interaction during pharmaceutical hot-melt extrusion. Eur J Pharm Biopharm 81:230–237

Saerens L, Vervaet C, Remon JP, De Beer T (2013a) Process monitoring and visualization solutions for hot-melt extrusion: a review. J Pharm Pharmacol. 66:180–203

Saerens L, Vervaet C, Remon J-P, De Beer T (2013b) Visualization and process understanding of material behavior in the extrusion barrel during a hot-melt extrusion process using raman spectroscopy. Anal Chem 85:5420–5429

Santovea A, Piero MJ, Llabres M (2010) Comparison between DSC and TMDSC in the investigation into frozen aqueous cryoprotectants solutions. Drug Dev Ind Pharm 36:1413–1421

Saxena A, Jean YC, Suryanarayanan R (2013) Annealing effect reversal by water sorption–desorption and heating above the glass transition temperature—comparison of properties. Mol Pharm 10:3005–3012

Schantz S, Hoppu P, Juppo AM (2009) A solid-state NMR study of phase structure, molecular interactions, and mobility in blends of citric acid and paracetamol. J Pharm Sci 98:1862–1870

Schmitt E, Davis CW, Long ST (1996) Moisture-dependent crystallization of amorphous lamotrigine mesylate. J Pharm Sci 85:1215–1219

Schönhals A Dielectric spectroscopy on the dynamics of amorphous polymeric systems. Novocontrol, Application note. http://novocontrol.de/pdf_s/APND1.PDF. Accessed 27 June 2013

Scoutaris N, Hook AL, Gellert PR, Roberts CJ, Alexander MR, Scurr DJ (2012) ToF-SIMS analysis of chemical heterogenities in inkjet micro-array printed drug/polymer formulations. J Mater Sci Mater Med 23:385–391

Seliger J, Žagar V (2013) Crystallization of an amorphous solid studied by nuclear quadrupole double resonance. Chem Phys 421:44–48

Shard AG, Rafati A, Ogaki R, Lee JLS, Hutton S, Mishra G, Davies MC, Alexander MR (2009) Organic depth profiling of a binary system: the compositional effect on secondary ion yield and a model for charge transfer during secondary Ion emission. J Phys Chem B 113:11574–11582

Shi Y, Zhang X-Y, Gong LL (2011) Molecular motion and detrapping behavior of trapped space charges in polyvinyl pyrrolidone: a thermally stimulated depolarization current study. Polym Bull 67:1595–1604

Shi P, Schach Rg, Munch E, Montes Hln, Lequeux Fo (2013) Glass transition distribution in miscible polymer blends: from calorimetry to rheology. Macromolecules 46:3611–3620

Shmeis R, Wang Z, Krill S (2004a) A mechanistic investigation of an amorphous pharmaceutical and its solid dispersions, Part I: a comparative analysis by thermally stimulated depolarization current and differential scanning calorimetry. Pharm Res 21:2025–2030

Shmeis R, Wang Z, Krill S (2004b) A mechanistic investigation of an amorphous pharmaceutical and its solid dispersions, Part II: Molecular mobility and activation thermodynamic parameters. Pharm Res 21:2031–2039

Sinclair W, Leane M, Clarke G, Dennis A, Tobyn M, Timmins P (2011) Physical stability and recrystallization kinetics of amorphous ibipinabant drug product by Fourier transform raman spectroscopy. J Pharm Sci 100:4687–4699

Sitterberg J, Özcetin A, Ehrhardt C, Bakowsky U (2010) Utilising atomic force microscopy for the characterisation of nanoscale drug delivery systems. Eur J Pharm Biopharm 74:2–13

Smith-Goettler B, Gendron CM, MacPhail N, Meyer RF, Phillips JX (2011) NIR monitoring of a hot-melt extrusion process. Spectrosc Lett

Song M, de Villiers MM, Redelinghuys A-M, Liebenberg W (2005) Isothermal and dynamic microcalorimetry for quantifying the crystallization of an amorphous drug during interactive powder mixing. Particul Sci Technol 23:323–334

Sousa LAE, Alem N, Beezer AE, Oâ €TM Neill MAA, Gaisford S (2010) Quantitative analysis of solid-state processes studied with isothermal microcalorimetry. J Phys Chem B 114:13173–13178

Soutari N, Buanz ABM, Gul MO, Tuleu C, Gaisford S (2012) Quantifying crystallisation rates of amorphous pharmaceuticals with dynamic mechanical analysis (DMA). Int J Pharm 423:335–340

Suknunthaa K, Jonesb DS, Tantishaiyakula V (2012) Properties of felodipine-poly (vinylpyrrolidone) solid dispersion films and the impact of solvents. Sci Asia 38:188–195

Sun Y, Tao J, Zhang GGZ, Yu L (2010) Solubilities of crystalline drugs in polymers: an improved analytical method and comparison of solubilities of indomethacin and nifedipine in PVP, PVP/VA, and PVAc. J Pharm Sci 99:4023–4031

Svoboda R, Málek Jr (2011) Interpretation of crystallization kinetics results provided by DSC. Thermochim Acta 526:237–251

Syll O, Richard B, Willart JF, Descamps M, Schuck P, Delaplace G, Jeantet R (2012) Rehydration behaviour and ageing of dairy powders assessed by calorimetric measurements. Innov Food Sci Emerg Technol 14:139–145

Szabó B, Süvegh K, Zelkó R (2011) Effect of storage on microstructural changes of Carbopol polymers tracked by the combination of positron annihilation lifetime spectroscopy and FT-IR spectroscopy. Int J Pharm 416:160–163

Szente V, Süvegh K, Marek T, Zelkó R (2009) Prediction of the stability of polymeric matrix tablets containing famotidine from the positron annihilation lifetime distributions of their physical mixtures. J Pharm Biomed Anal 49:711–714

Tarek El G, Roland Bh (2007) Dielectric relaxation processes in solid and supercooled liquid solutions of acetaminophen and nifedipine. J Phys Condens Matter 19:205134

Tatton AS, Pham TN, Vogt FG, Iuga D, Edwards AJ, Brown SP (2013) Probing hydrogen bonding in cocrystals and amorphous dispersions using ^{14}N–^{1}H HMQC solid-State NMR. Mol Pharm 10:999–1007

Taylor LS, Langkilde FW, Zografi G (2001) Fourier transform Raman spectroscopic study of the interaction of water vapor with amorphous polymers. J Pharm Sci 90:888–901

Thielmann F, Levoguer C (2002) iGC-A new instrumental technique for characterising the phyisco-chemical properties of pharmaceutical materials. Application note 301

Tobyn M, Brown J, Dennis AB, Fakes M, Gao Q, Gamble J, Khimyak YZ, McGeorge G, Patel C, Sinclair W, Timmins P, Yin S (2009) Amorphous drug–PVP dispersions: application of theoretical, thermal and spectroscopic analytical techniques to the study of a molecule with intermolecular bonds in both the crystalline and pure amorphous state. J Pharm Sci 98:3456–3468

Toth SJ, Madden JT, Taylor LS, Marsac P, Simpson GJ (2012) Selective imaging of active pharmaceutical ingredients in powdered blends with common excipients utilizing two-photon excited ultraviolet-fluorescence and ultraviolet-second order nonlinear optical imaging of chiral crystals. Anal Chem 84:5869–5875

Trasi N, Byrn S (2012) Mechanically induced amorphization of drugs: a study of the thermal behavior of cryomilled compounds. AAPS PharmSciTech 13:772–784
Trasi N, Boerrigter SM, Byrn S (2010) Investigation of the milling-induced thermal behavior of crystalline and amorphous griseofulvin. Pharm Res 27:1377–1389
Tumuluri VS, Kemper MS, Lewis IR, Prodduturi S, Majumdar S, Avery BA, Repka MA (2008) Off-line and on-line measurements of drug-loaded hot-melt extruded films using Raman spectroscopy. Int J Pharm 357:77–84
Urbanova M, Brus J, Sedenkova I, Policianova O, Kobera L (2013) Characterization of solid polymer dispersions of active pharmaceutical ingredients by ^{19}F MAS NMR and factor analysis. Spectrochim Acta A 100:59–66
USFDA (2012) http://www.accessdata.fda.gov/scripts/cdrh/cfdocs/cfcfr/CFRsearch.cfm?CFRPart=314. Accessed 18 Jan 2014
Van den Mooter G (2012) The use of amorphous solid dispersions: a formulation strategy to overcome poor solubility and dissolution rate. Drug Discov Today Technol 9:e79–e85
van Drooge DJ, Braeckmans K, Hinrichs WLJ, Remaut K, De Smedt SC, Frijlink HW (2006a) Characterization of the mode of incorporation of lipophilic compounds in solid dispersions at the nanoscale using fluorescence resonance energy transfer (FRET). Macromol Rapid Commun 27:1149–1155
van Drooge DJ, Hinrichs WLJ, Visser MR, Frijlink HW (2006b) Characterization of the molecular distribution of drugs in glassy solid dispersions at the nano-meter scale, using differential scanning calorimetry and gravimetric water vapour sorption techniques. Int J Pharm 310:220–229
Van Eerdenbrugh B, Taylor LS (2011) Application of mid-IR spectroscopy for the characterization of pharmaceutical systems. Int J Pharm 417:3–16
Vassilikou-Dova A, Kalogeras IM (2008) Dielectric analysis (DEA), thermal analysis of polymers. Wiley, pp 497–613
Vehring R, Ivey J, Williams L, Joshi V, Dwivedi S, Lechuga-Ballesteros D, Dalby RN, Byron PB, Peart J, Suman JD (2012) High-sensitivity analysis of crystallinity in respirable powders using low frequency shift-Raman spectroscopy. Respir Drug Deliv 2:641–644
Viciosa T, Pires G, Ramos JJM (2009) Revisitation of the molecular mobility of the amorphous solid 4,4′-methylenebis (N, N-diglycidylaniline) (MBDA): new contributions from the TSDC technique. J Mol Liquids 148:114–119
Vitez IM, Newman AW, Davidovich M, Kiesnowski C (1998) The evolution of hot-stage microscopy to aid solid-state characterizations of pharmaceutical solids. Thermochim Acta 324:187–196
Voelkel A, Strzemiecka B, Adamska K, Milczewska K (2009) Inverse gas chromatography as a source of physiochemical data. J Chromatogr A 1216:1551–1566
Vogt FG, Williams GR (2010) Advanced approaches to effective solid-state analysis: X-ray diffraction, vibrational spectroscopy and solid-state NMR. Am Pharm Rev 13:1–17
Vogt F, Williams G (2012) Analysis of a nanocrystalline polymer dispersion of ebselen using solid-state NMR, Raman microscopy, and powder X-ray diffraction. Pharm Res 29:1866–1881
Vogt FG, Clawson JS, Strohmeier M, Pham TN, Watson SA, Edwards AJ, Gad SC (2011) New approaches to the characterization of drug candidates by solid-state NMR, Pharmaceutical Sciences Encyclopedia. Wiley
Vogt FG, Yin H, Forcino RG, Wu L (2013) ^{17}O Solid-state NMR as a sensitive probe of hydrogen bonding in crystalline and qmorphous solid forms of diflunisal. Mol Pharm 10:3433–3446
Vyazovkin S, Dranca I (2006) Probing beta relaxation in pharmaceutically relevant glasses by using DSC. Pharm Res 23:422–428
Vyazovkin S, Dranca I (2007) Effect of physical aging on nucleation of amorphous indomethacin. J Phys Chem B 111:7283–7287
Wahl PR, Treffer D, Mohr S, Roblegg E, Koscher G, Khinast JG (2013) Inline monitoring and a PAT strategy for pharmaceutical hot melt extrusion. Int J Pharm 455:159–168
Wanapun D, Kestur US, Taylor LS, Simpson GJ (2011) Single particle nonlinear optical imaging of trace crystallinity in an organic powder. Anal Chem 83:4745–4751

Wang L-M, Velikov V, Angell CA (2002) Direct determination of kinetic fragility indices of glass-forming liquids by differential scanning calorimetry: kinetic versus thermodynamic fragilities. J Chem Phys 117:10184

Wegiel LA, Mauer LJ, Edgar KJ, Taylor LS (2012) Mid-infrared spectroscopy as a polymer selection tool for formulating amorphous solid dispersions. J Pharm Pharmacol. doi:10.1111/jphp.12079

Weinberg MC, Birnie I DP, Shneidman VA (1997) Crystallization kinetics and the JMAK equation. J Non-Cryst Solids 219:89–99

Weuts I, Kempen D, Verreck G, Peeters J, Brewster M, Blaton N, Van den Mooter G (2005) Salt formation in solid dispersions consisting of polyacrylic acid as a carrier and three basic model compounds resulting in very high glass transition temperatures and constant dissolution properties upon storage. Eur J Pharm Sci 25:387–393

Willart J-F, Carpentier L, Danède F, Descamps M (2012) Solid-state vitrification of crystalline griseofulvin by mechanical milling. J Pharm Sci 101:1570–1577

Williams G (2009) Chain dynamics in solid polymers and polymerizing systems as revealed by broadband dielectric spectroscopy. Macromol Symp 286:1–19

Winkel K, Bowron DT, Loerting T, Mayer E, Finney JL (2009) Relaxation effects in low density amorphous ice: two distinct structural states observed by neutron diffraction. J Chem Phys 130:204502

Wojnarowska Z, Grzybowska K, Adrjanowicz K, Kaminski K, Paluch M, Hawelek L, Wrzalik R, Dulski M, Sawicki W, Mazgalski J, Tukalska A, Bieg T (2010) Study of the amorphous glibenclamide drug: analysis of the molecular dynamics of quenched and cryomilled material. Mol Pharm 7:1692–1707

Wyttenbach N, Janas C, Siam M, Lauer ME, Jacob L, Scheubel E, Page S (2013) Miniaturized screening of polymers for amorphous drug stabilization (SPADS): rapid assessment of solid dispersion systems. Eur J Pharm Biopharm 84:583–598

Yang M, Gogos C (2013) Crystallization of poly(ethylene oxide) with acetaminophen-A study on solubility, spherulitic growth, and morphology. Eur J Pharm Biopharm 85:889–897

Yang J, Grey K, Doney J (2010) An improved kinetics approach to describe the physical stability of amorphous solid dispersions. Int J Pharm 384:24–31

Yang M, Wang P, Suwardie H, Gogos C (2011) Determination of acetaminophen's solubility in poly(ethylene oxide) by rheological, thermal and microscopic methods. Int J Pharm 403:83–89

Yang Z, Nollenberger K, Albers J, Craig D, Qi S (2013) Microstructure of an immiscible polymer blend and its stabilization effect on amorphous solid dispersions. Mol Pharm 10:2767–2780

Yonemochi E, Inoue Y, Buckton G, Moffat A, Oguchi T, Yamamoto K (1999) Differences in crystallization behavior between quenched and ground amorphous ursodeoxycholic acid. Pharm Res 16:835–840

Yoshihashi Y, Iijima H, Yonemochi E, Terada K (2006) Estimation of physical stability of amorphous solid dispersion using differential scanning calorimetry. J Therm Anal Calorim 85:689–692

Yoshihashi Y, Yonemochi E, Maeda Y, Terada K (2010) Prediction of the induction period of crystallization of naproxen in solid dispersion using differential scanning calorimetry. J Therm Anal Calorim 99:15–19

Young PM, Chiou H, Tee T, Traini D, Chan H-K, Thielmann F, Burnett D (2007) The use of organic vapor sorption to determine low levels of amorphous content in processed pharmaceutical powders. Drug Dev Ind Pharm 33:91–97

Yuan X, Carter BP, Schmidt SJ (2011) Determining the critical relative humidity at which the glassy to rubbery transition occurs in polydextrose using an automatic water vapor sorption instrument. J Food Sci 76:E78–E89

Zeitler JA, Taday PF, Newnham DA, Pepper M, Gordon KC, Rades T (2007) Terahertz pulsed spectroscopy and imaging in the pharmaceutical—a review. J Pharm Pharmacol 59:209–223

Zelkóa Rn, Orbán Ãdm, Süvegh Kr (2006) Tracking of the physical ageing of amorphous pharmaceutical polymeric excipients by positron annihilation spectroscopy. J Pharm Biomed Anal 40:249–254

Zhang S, Painter PC, Runt J (2004) Suppression of the dielectric secondary relaxation of poly(2-vinylpyridine) by strong intermolecular hydrogen bonding. Macromolecules 37:2636–2642
Zhang J, Bunker M, Chen X, Parker AP, Patel N, Roberts CJ (2009) Nanoscale thermal analysis of pharmaceutical solid dispersions. Int J Pharm 380:170–173
Zhuravlev E, Schick C (2010) Fast scanning power compensated differential scanning nano-calorimeter: 2. Heat capacity analysis. Thermochim Acta 505:14–21
Zidan AS, Rahman Z, Sayeed V, Raw A, Yu L, Khan MA (2012) Crystallinity evaluation of tacrolimus solid dispersions by chemometric analysis. Int J Pharm 423:341–350